ACS OMEGA

http://pubs.acs.org/journal/acsodf

Article

Polymeric Nanoparticles with a Sera-Derived Coating for Efficient Cancer Cell Uptake and Killing

Daniel Nierenberg,[⊥] Orielyz Flores,[⊥] David Fox, Yuen Yee Li Sip, Caroline Finn, Heba Ghozlan, Amanda Cox, K. Kai McKinstry, Lei Zhai, and Annette R. Khaled*

Cite This: *ACS Omega* 2021, 6, 5591−5606

Read Online

ACCESS | Metrics & More | Article Recommendations | Supporting Information

ABSTRACT: Nanoparticle-mediated cancer drug delivery remains an inefficient process. The protein corona formed on nanoparticles (NPs) controls their biological identity and, if optimized, could enhance cancer cell uptake. In this study, a hyperbranched polyester polymer (HBPE) was synthesized from diethyl malonate and used to generate NPs that were subsequently coated with normal sera (NS) collected from mice. Cellular uptake of NS-treated HBPE-NPs was compared to PEGylated HBPE-NPs and was assessed using MDA-MB-231 triple-negative breast cancer (TNBC) cells as well as endothelial and monocytic cell lines. NS-treated HBPE-NPs were taken up by TNBC cells more efficiently than PEGylated HBPE-NPs, while evasion of monocyte uptake was comparable. NS coatings facilitated cancer cell uptake of HBPE-NPs, even after prior interaction of the particles with an endothelial layer. NS-treated HBPE-NPs were not inherently toxic, did not induce the migration of endothelial cells that could lead to angiogenesis, and could efficiently deliver cytotoxic doses of paclitaxel (taxol) to TNBC cells. These findings suggest that HBPE-NPs may adsorb select sera proteins that improve uptake by cancer cells, and such NPs could be used to advance the discovery of novel factors that improve the bioavailability and tissue distribution of drug-loaded polymeric NPs.

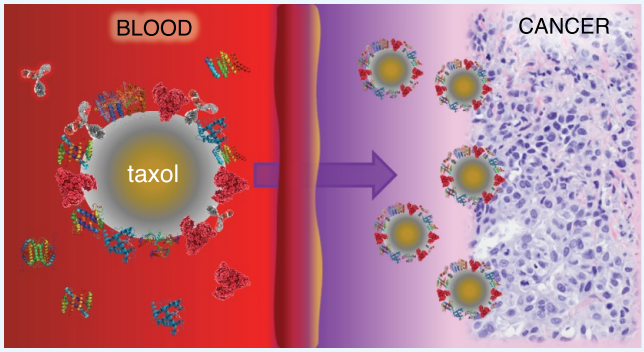

INTRODUCTION

Advances in nanotechnology hold promises for improving anticancer drug efficacy by delivering therapeutic cargo specifically to disease sites. However, achieving effective local accumulation of nanocarriers in tumors remains a challenge. Various strategies are ongoing to enhance the intratumoral concentration of nanomedicines. Taking advantage of the enhanced permeability and retention (EPR) effect, due to abnormal leakage of tumor vessels, is one approach for the passive targeting of nanomedicines.[1] However, gaps between endothelial cells may not be responsible for the movement of particles from the vasculature into tumors,[2] in part explaining why current approaches for nanoparticle drug delivery to cancer cells result in efficiencies as low as 0.0014%.[3,4] The rapid removal of circulating NPs by the reticuloendothelial system (RES) is another factor that reduces tumor accumulation of systemically introduced nanomedicines.[5] Antifouling approaches like the use of poly(ethylene glycol) (PEG) to modify the surface of NPs are used to enhance biocompatibility and increase circulation time.[6] But the repeated administration of PEG-modified NPs could cause production of anti-PEG antibodies as part of the host immune response against PEGylated nanomedicines.[7] The PEG density and chain length are also factors that could hinder cancer cell uptake.[8] Hence identifying novel antibiofouling coatings that are not immunogenic is needed to overcome the limitations of current nanocarriers.

An emerging strategy for targeting NPs to tumors is modifying the nanoparticle surface to promote interactions with biological components that naturally target specific cells. In the presence of fluids like blood or cell culture media, NPs adsorb biomolecules forming what has been termed a "corona".[9] This corona is composed of proteins and possibly other biological molecules like lipids. A protein corona is likely formed by two distinct layers: a hard corona made from proteins with a strong affinity for the nanoparticle surface and a soft corona consisting of proteins that may transiently interact with NPs. The formation of a protein corona remodels the nanobio interface and is thus a major factor in defining the pharmacological profile of nanomedicines.[10] Key parameters such as blood circulation time, tissue biodistribution,

Received: December 9, 2020
Accepted: February 11, 2021
Published: February 19, 2021

https://dx.doi.org/10.1021/acsomega.0c05998
ACS Omega 2021, 6, 5591−5606

Scheme 1. Synthesis Schematic for HBPE Polymer[a]

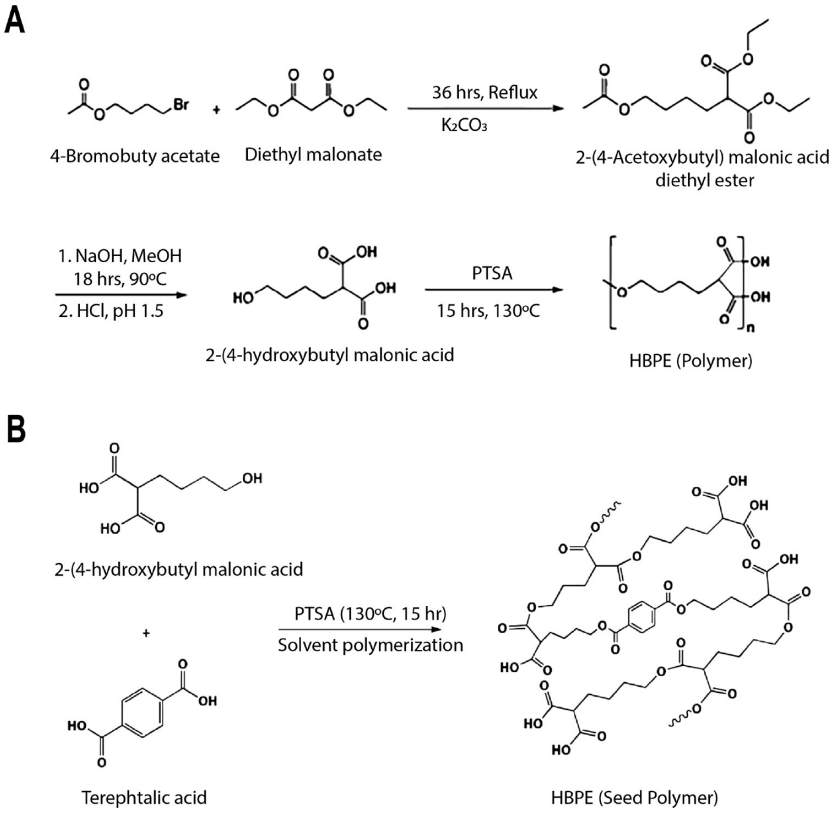

[a](A) BBA, DEM, and K_2CO_3 reactants were dissolved in acetonitrile in molar ratios of 1, 1.1, and 1, respectively. After 36 h under reflux, the 2-(4-Acetoxybutyl) malonic acid diethyl ether product (compound **1**) was purified by separatory funnel extraction, rotary evaporation, and vacuum distillation. Oxygen-bound end groups were deprotected with NaOH and protonated with HCl. The monomer product (compound **2**) was purified through vacuum distillation and rotary evaporation. The monomer was then polymerized with a (PTSA) acid catalyst in a DMSO solvent under an inert nitrogen atmosphere. For polymerization, the monomer was dispensed in solution with a syringe pump at a 0.1 mL per hour rate. (B) For seed-based polymerization, all synthesis steps were identical to non-seed HBPE polymerization apart from the following. After compound **2** purification, the monomer was then polymerized with the PTSA catalyst and a terephthalic acid seed in the DMSO solvent under an inert nitrogen atmosphere.

biodegradation, hemocompatibility, toxicity, and others are affected by the biomolecules that form a protein corona on NPs.[10] Such findings are the foundation for strategies to produce biomimetic NPs that integrate biological elements in nanoformulations. As an example, use of cell membrane-coated NPs was first examined using membranes from red blood cells (RBCs).[11] Unlike PEGylation that is a "bottom-up" approach, coating NPs with cell membranes utilizes a "top-down" approach that is more facile and endows NPs with the characteristics of the cell membrane donor cell.[12,13] In addition to RBCs, various other cell types can provide membranes to coat NPs, such stem cells, leukocytes, platelets, or cancer cells. Despite advantages in immune evasion, improved biodistribution and circulation time, enhanced natural targeting, and being eco-friendly, the translation of cell membrane coating nanotechnology from the lab to the clinic remains challenging.[14−16] There are unresolved issues with standardization of membrane source cells and large-scale production. The identity of the essential membrane proteins that improve tumor targeting of coated NPs is poorly characterized, which impedes reproducibility. Additionally, inherent problems exist with the use of RBCs and platelets, such as the lack of tumor targeting and the need for donor blood, and carcinogenic risk associated with cancer cells or exosomes.[17]

An ideal solution would be coating NPs with an optimal combination of proteins that confer a biological identity to the nanomedicines that is amenable to tumor accumulation. However, the knowledge needed to create such a nanoparticle coating is lacking. Increasing our understanding of the interaction of NPs with biomolecules is essential to advance the clinical application of biomimetic approaches for nanomedicines. The NPs themselves may be a key to achieve this end. If NPs selectively adsorb proteins and other biomolecules from surrounding fluid, these particles can enrich for high and low abundance factors important in the manipulation of the biointerface that can be used to improve the targeting of nanomedicines to disease sites. This rational is supported by the reported use of NPs as probes to detect disease.[18,19] Moreover, the physio-chemical features of NPs such the size, shape, or hydrophobicity can be further modified to modulate corona formation and thereby lead to the identification of novel proteins that enhance the tumor targeting of nanomedicines.[20]

In this study, we use NPs formulated with a novel aliphatic and malonate-based synthetic polymer termed HBPE[21−23] to investigate the effect of a serum-based protein corona on breast cancer cell uptake and drug delivery as compared to PEGylation. We previously found that the three-dimensional (3D), globular HBPE polymer forms amphiphilic polymeric

https://dx.doi.org/10.1021/acsomega.0c05998
ACS Omega 2021, 6, 5591−5606

cavities for effective encapsulations of hydrophobic drug cargos. In the intracellular environment (e.g., esterases, acidic pH), the presence of ester linkages in the polymeric backbone yields small chain (2−5 carbon) length alcohols and weak acids. Such degradation byproducts are easily excluded from the body by the renal system as shown for other degradable polymers.[24] This results in minimal toxicity and higher biocompatibility when HBPE-NPs are used *in vivo*. A synthetic polymer such as HBPE is also preferable to polymers formed using natural sugars, like chitosan,[25] since synthesis is more reproducible and less likely to stimulate the immune system. Unlike other hyperbranched aliphatic polyesters, such as poly(glycolide) (PGA) that lacks functional groups on the polymer backbone,[26,27] the HBPE polymer forms carboxylated (COOH)-functionalized NPs that can be further functionalized using carbodiimide chemistry. Importantly, the HBPE polymer, unlike dendrimers, can be synthesized in one-pot and does not need multiple iterative steps.[23,28] In aqueous solutions, the HBPE polymer self-assembles, with the hydrophobic areas internalizing, while exposing the hydrophilic areas containing the polar carboxylic acid groups. This property, unlike micro-emulsion methods, enables encapsulation of hydrophobic drug cargos using a water-based solvent diffusion method and is an advantageous feature of the HBPE polymer along with the capacity for surface functionalization, solubility in common polar solvents, and selective biodegradability at low-pH or under enzymatic conditions.

Due the described features of HBPE-NPs, these particles could potentially be an ideal platform for the enrichment and subsequent identification of biomolecules that facilitate tumor accumulation. In support, our published studies demonstrated that HBPE-based NPs delivered a hydrophobic peptide called CT20p *in vitro* and *in vivo* to tumor cells that led to cancer cell killing and tumor regression.[21,22,29−31] Thus, we surmise that HBPE-NPs form a corona containing critical proteins that enhance the tumor accumulation of particles. To investigate this, we performed comparisons of the uptake of NS-treated HBPE-NPs and PEGylated (PEG) HBPE-NPs using monocytic, endothelial, and cancer cell lines. A novel endothelial cell-based transwell assay was used to determine whether a preformed protein corona on HBPE-NPs could modulate interactions with an endothelial layer and then be subsequently taken up by cancer cells. Findings support that HBPE-NPs adsorb select sera components that enhance delivery of anticancer agents to tumor cells. Hence, HBPE-NPs can serve as a source for the discovery of new factors that, when used to coat NPs, will optimize the biological behavior of nanomedicines by positively influencing cancer cell-targeting capacity.

RESULTS

Optimization of Synthesis of HBPE Polymer and Characterization of HBPE-NPs. To address challenges with the delivery of cancer drugs to tumors, we synthesized the HBPE polymer (Scheme 1A) based on the work reported by Santra et al.[23,28,32] An advantageous feature of the HBPE polymer is its aliphatic nature, consisting of hydrophilic carboxylic acids on its surface and hydrophobic hydrocarbons in its core. This property permits hydrophilic and hydrophobic drug encapsulation within the polymer's inner pores, facilitating solubility in aqueous environments. The AB_2 monomer is designed to grow in three dimensions during polymerization, to form a highly branched polymer. The degree of polymerization of the HBPE monomer, and in turn its diameter and branching, can be altered through changes in reaction time during the synthesis, allowing for adjustment in the polymer pore size to optimize drug encapsulation. In previous studies, we employed HBPE-NPs for delivery of a therapeutic peptide to regress breast and prostate tumors in mice.[22,29,31] However, these studies also showed that our particles, even when PEGylated, were also taken up by the liver and spleen, which reduced bioavailability (Figure 1). Since

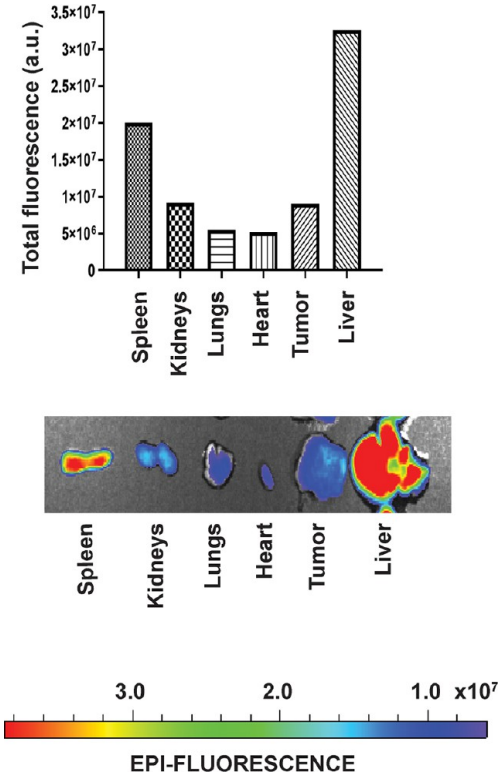

Figure 1. PEGylated HBPE-NPs accumulate in liver, spleen, and tumor, respectively. Shown are bar graphs for total organ fluorescence quantification (upper panel) and organ imaging (lower panel) 7 h post-treatment of tumor-bearing mice intravenously injected with DiR dye-loaded PEGylated HBPE-PEG-NPs. Nu/Nu nude mouse was orthotopically injected with 8×10^5 MDA-MB-231 TNBC cells in the mammary fat pad. Images were taken with an IVIS Lumina S5 and quantified with Living Image software. Images represent HBPE-PEG-NP uptake (DiR fluorescence) in the spleen, kidneys, lungs, heart, tumor, and liver.

NPs of uniform size and shape are ideal for cargo delivery to cells,[33] we optimized HBPE polymer synthesis to achieve a uniform nanoparticle diameter and dispersity in several ways. First, in the monomer synthesis steps, column chromatography was replaced by vacuum distillation to reduce the synthesis time and increase the product yield of compounds 1 and 2 (Scheme 1A). Second, the hydrochloric acid (HCl) concentration and dispersion rate were reduced to improve compound **2** recovery. Lastly, for polymerization, the solvent volume was increased, and the monomer was added dropwise to the solvent through a syringe pump at specific amounts and time intervals. Variants of this approach were tested to optimize branching of the polymer, which controls the polymer molecular weight (MW) and resulting particle size and cargo-loading capacity. Two methods were evaluated: the slow addition of monomer[34,35] and the use of terephthalic acid

https://dx.doi.org/10.1021/acsomega.0c05998
ACS Omega 2021, 6, 5591−5606

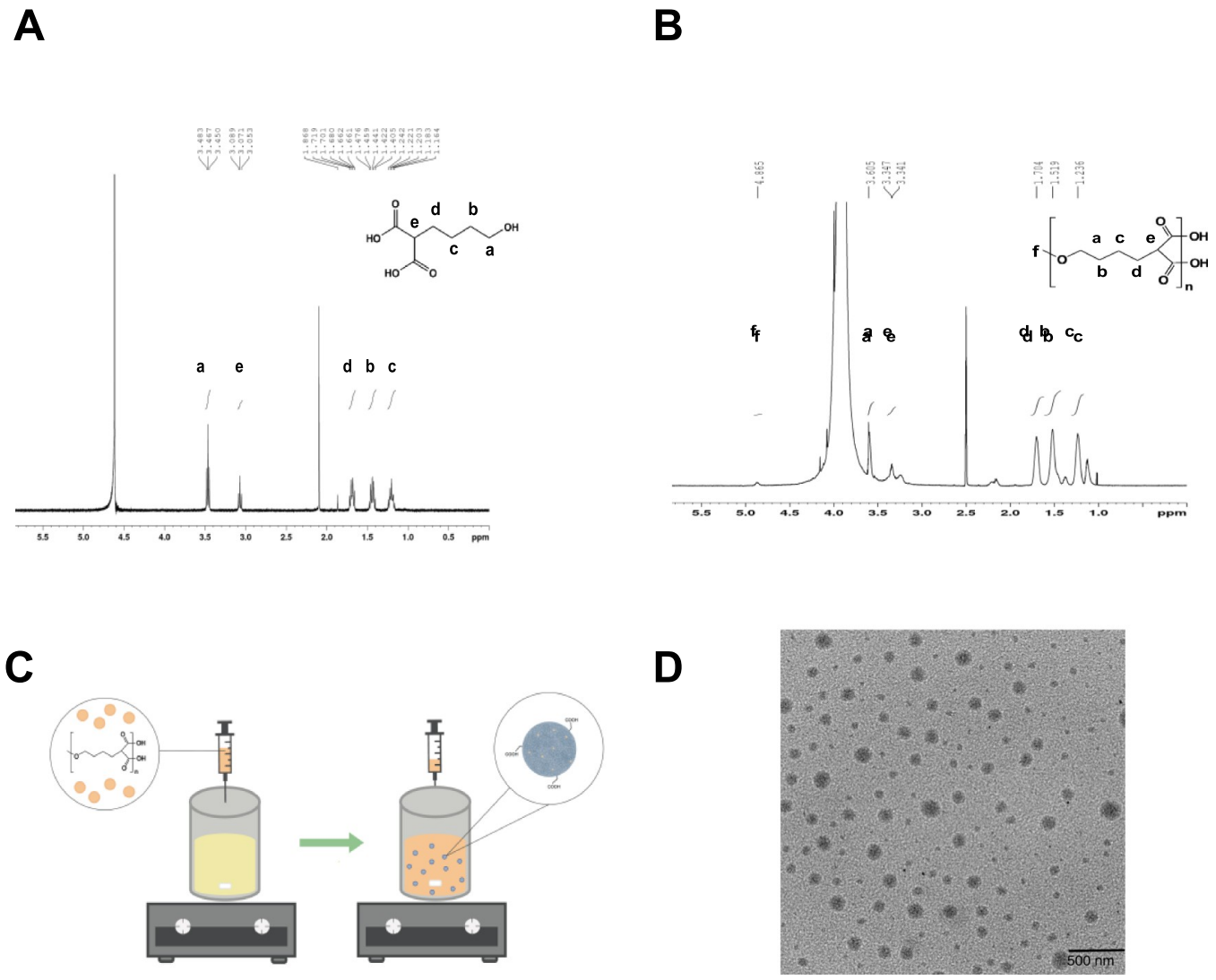

Figure 2. HBPE polymer forms monodispersed NPs. (A, B) Hydrogen nuclear magnetic resonance (^{1}H NMR) spectra of (A) monomer (compound **2**) and (B) HBPE polymer. (C) Schematic of the solvent diffusion method for producing HBPE-NPs and encapsulating cargo. (D) TEM images of COOH-HBPE-NPs to assess dispersity and morphology. Images were acquired with a JEOL TEM-011 microscope.

(1:20 ratio to monomer) as a seed for polymerization (Scheme 1B).[36]

Nuclear magnetic resonance (^{1}H NMR) results for the HBPE monomer and polymer showed expected findings based on previously reported data[23] (result for the slow addition method shown, Figure 2A,B). Distinct peaks were observed with the correct number of segmentations and chemical shifts (ppm) for each hydrogen type, indicating successful monomer synthesis. After polymerization, NMR peaks widened and peak segmentation reduced, signifying monomer branching. To track NPs in cells or *in vivo*, fluorescent hydrophobic probes, 1,1′-dioctadecyl-3,3,3′,3′-tetramethylindocarbocyanine perchlorate (DiI) or 1,1′-dioctadecyl-3,3,3′,3′-tetramethylindotricarbocyanine iodide (DiR) was encapsulated within the HBPE-NPs as appropriate for detection. For dye encapsulation, the solvent diffusion method was used (schematic, Figure 2C). We confirmed that all NPs had equivalent loading of dye by fluorometry (Figure S1A). After dye-encapsulated NPs were formed, nanoparticle morphology, dispersity, and diameter were evaluated to ensure that NPs of uniform size and shape were produced. To examine this, transmission electron microscopy (TEM) was performed (Figure 2D). Anhydrous NPs displayed a spherical and monodispersed nature and ranged in a diameter between 100 and 160 nm, demonstrating that syringe pump-mediated control over polymerization was achieved. To evaluate the hydrodynamic nanoparticle diameter, dynamic light scattering (DLS) was performed (Table 1).

Table 1. DLS Data for NPs Made from HBPE Polymer[a]

nanoparticle	particle size (nm ± σ)	PDI ± σ	ζ-potential (mV ± σ)
COOH-HBPE-NPs	160.1 ± 2.5	0.145 ± 0.068	−39.1 ± 0.9
$COOH_{(s)}$-HBPE-NPs	159.0 ± 2.7	0.147 ± 0.040	−40.2 ± 1.5

[a](s) terephthalic acid seed-based polymer; PDI, polydispersity index.

COOH-HBPE-NPs showed an average diameter, dispersity (polydispersity index (PDI)), and zeta (ζ) potentials of 160 nm, 0.146, and −39 mV, respectively, indicating a desired diameter, stability, and dispersity consistent with our labs' previous studies.[23,31]

Protein Corona Formation and Inherent Toxicity of HBPE-NPs. An important factor influencing the biological

https://dx.doi.org/10.1021/acsomega.0c05998
ACS Omega 2021, 6, 5591−5606

Table 2. DLS Data for HBPE-NPs Treated with NS[a]

nanoparticle	particle size (nm ± σ)	PDI ± σ
COOH-HBPE-NPs	162.2 ± 3.8	0.185 ± 0.034
COOH-HBPE-NPs + anti-IgG	146.7 ± 3.9	0.182 ± 0.022
PEG-HBPE-NPs	224.6 ± 8.1	0.237 ± 0.004
PEG-HBPE-NPs + anti-IgG	206.1 ± 0.5	0.208 ± 0.025
COOH-HBPE-NPs + 5% NS	152.7 ± 3.0	0.123 ± 0.040
COOH-HBPE-NPs + 5% NS + anti-IgG	187.4 ± 1.8	0.095 ± 0.015

[a]PDI, polydispersity index.

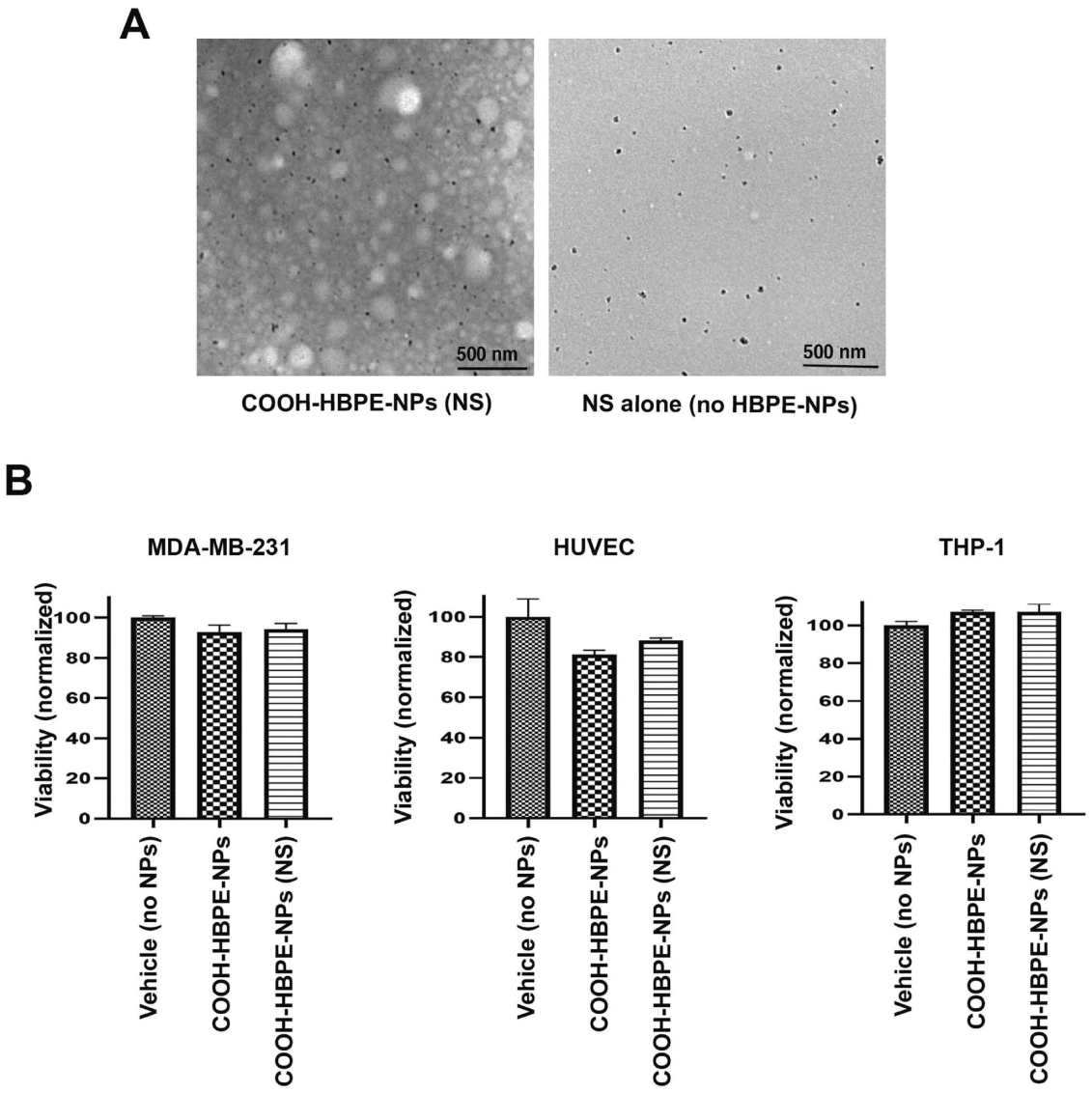

Figure 3. HBPE-NPs that form sera-derived protein corona are non-toxic. (A) TEM images of NS-treated COOH-HBPE-NPs (left panel) and NS alone (right panel). NPs were incubated with sera in a 20:1 volumetric ratio for 15 min. Images were acquired with a JEOL TEM-011 microscope. (B) TNBC MDA-MB-231 cells (left panel), endothelial HUVECs (mid panel), and monocytic THP-1 cells (right panel) were treated with a vehicle (water), COOH-HBPE-NPs, and NS-coated COOH-HBPE-NPs for 24 h of treatment. Cell viability was assessed using an MTT assay. Data in graph displays mean ± standard deviation (n = 3).

identity of NPs is the formation of the protein corona. NPs can adsorb distinct proteins from biological fluids like cell culture media or sera, which in turn affect biodistribution when systemically applied. To study this, we evaluated the coronae formed on HBPE-NPs treated with mouse NS. A 5% volume-to-volume (or 20:1) ratio of NS to nanoparticle was used to coat HBPE-NPs. The sera-to-nanoparticle ratio and incubation time were determined by assessing the minimum sera volume and incubation time that allowed for a noticeable change in DLS diameter values upon sera addition to HBPE-NPs.[37,38] To verify the presence of a protein corona, the nanoparticle size was measured before and after NS exposure using DLS (Table 2). COOH-HBPE-NPs and PEGylated (PEG-HBPE-NPs)

https://dx.doi.org/10.1021/acsomega.0c05998
ACS Omega 2021, 6, 5591−5606

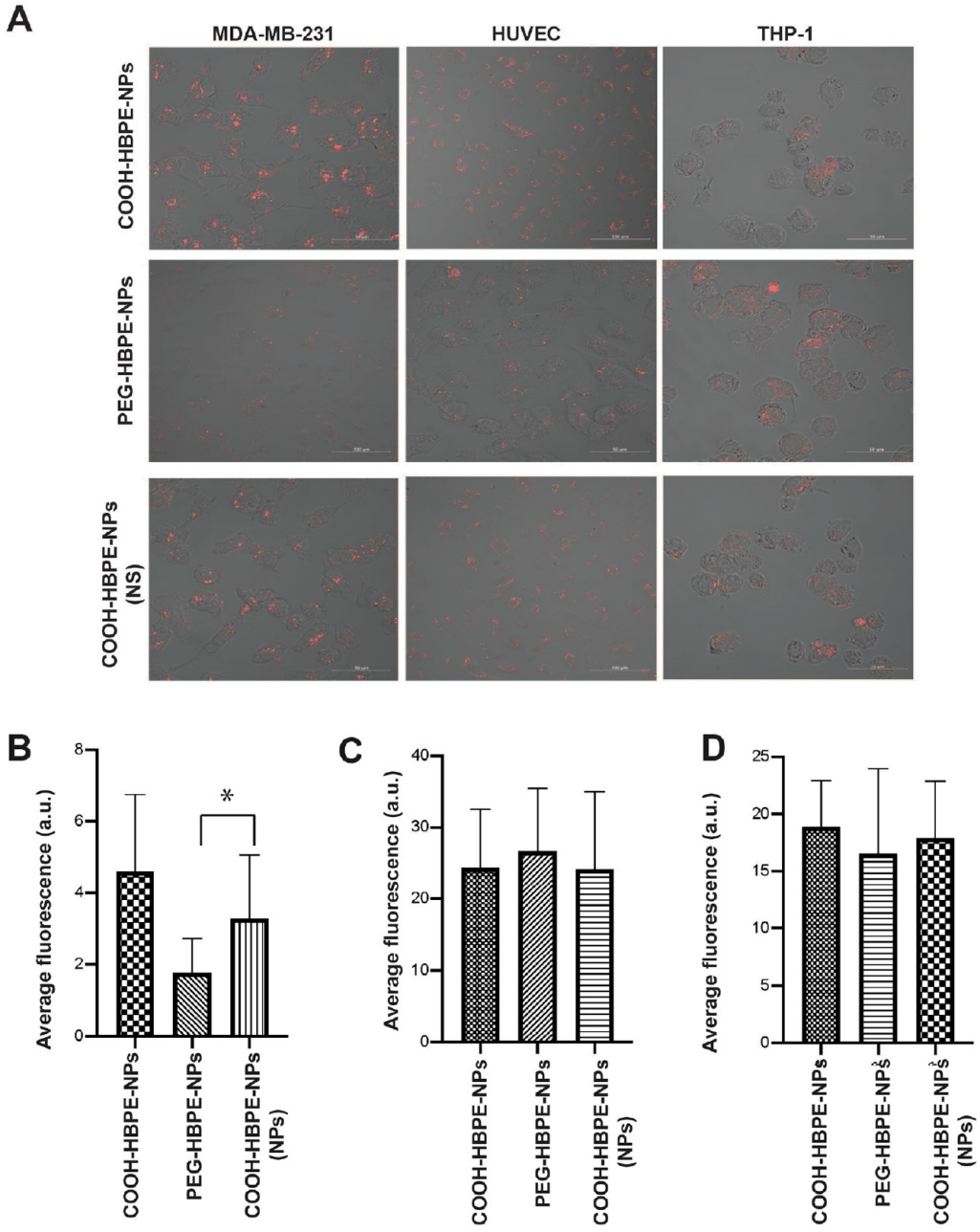

Figure 4. Pretreatment with NS improves cancer cell uptake of HBPE-NPs. (A) Representative confocal microscopy nanoparticle uptake images (single cell plane) of MDA-MB-231 cells (left column), HUVECs (middle column), and THP-1 cells (right column) treated with DiI dye-encapsulated COOH-HBPE-NPs (top row), PEG-HBPE-NPs (middle row), and NS-treated COOH-HBPE-NP (bottom row). Scale bar represents 50, 200, and 50 μm for MDA-MB-231, HUVEC, and THP-1 cells, respectively. Images were taken with a Zeiss LSM 710 microscope at 40× (MDA-MB-231 and THP-1 cells) and 20× (HUVECs) magnification. (B–D) Bar graphs represent average DiI fluorescence per cell. MDA-MB-231 cells (B), HUVECs (C), and THP-1 cells (D) were treated with COOH-HBPE-NP, PEG-HBPE-NPs, or NS-treated COOH-HBPE-NP (HS) for 24 h. Imaging was performed with a Cytation 5 cell imaging multi-mode reader (see Figure S3 for representative images). MDA-MB-231 and HUVEC fluorescence data was acquired from 100 cells. THP-1 fluorescence data was acquired from a total of 50 cells. Fluorescence was quantified using ZEN blue software. Data represents mean ± standard deviation. *p-value <0.0001 relative to PEG-HBPE-NPs. Representative data from three replicates is shown.

NPs were compared to assess the difference in nanoparticle surface modification upon corona formation.

After NS treatment, COOH-HBPE-NPs decreased in average diameter by ∼5.8%. The size reduction of the HBPE-NPs could be due to proteins in the NS interacting with the particle hydrophobic core and causing the branching of the HBPE polymer to constrict.[39,40] To confirm that diameter changes in HBPE-NPs were due to adsorption of coronal proteins from NS, anti-IgG antibodies were employed using a protocol adopted from Zheng et al. to detect the immunoglobulin IgG associated with NPs.[37] In principle, when HBPE-NPs capture sera proteins, such as IgG, antibodies to IgG will bind to the serum protein, increasing the size of the HBPE-NPs, which can be detected by DLS. After anti-IgG antibody addition, NS-treated COOH-HBPE-NPs increased in average diameter by ∼22.7%, respectively, as compared to NS-

https://dx.doi.org/10.1021/acsomega.0c05998
ACS Omega 2021, 6, 5591−5606

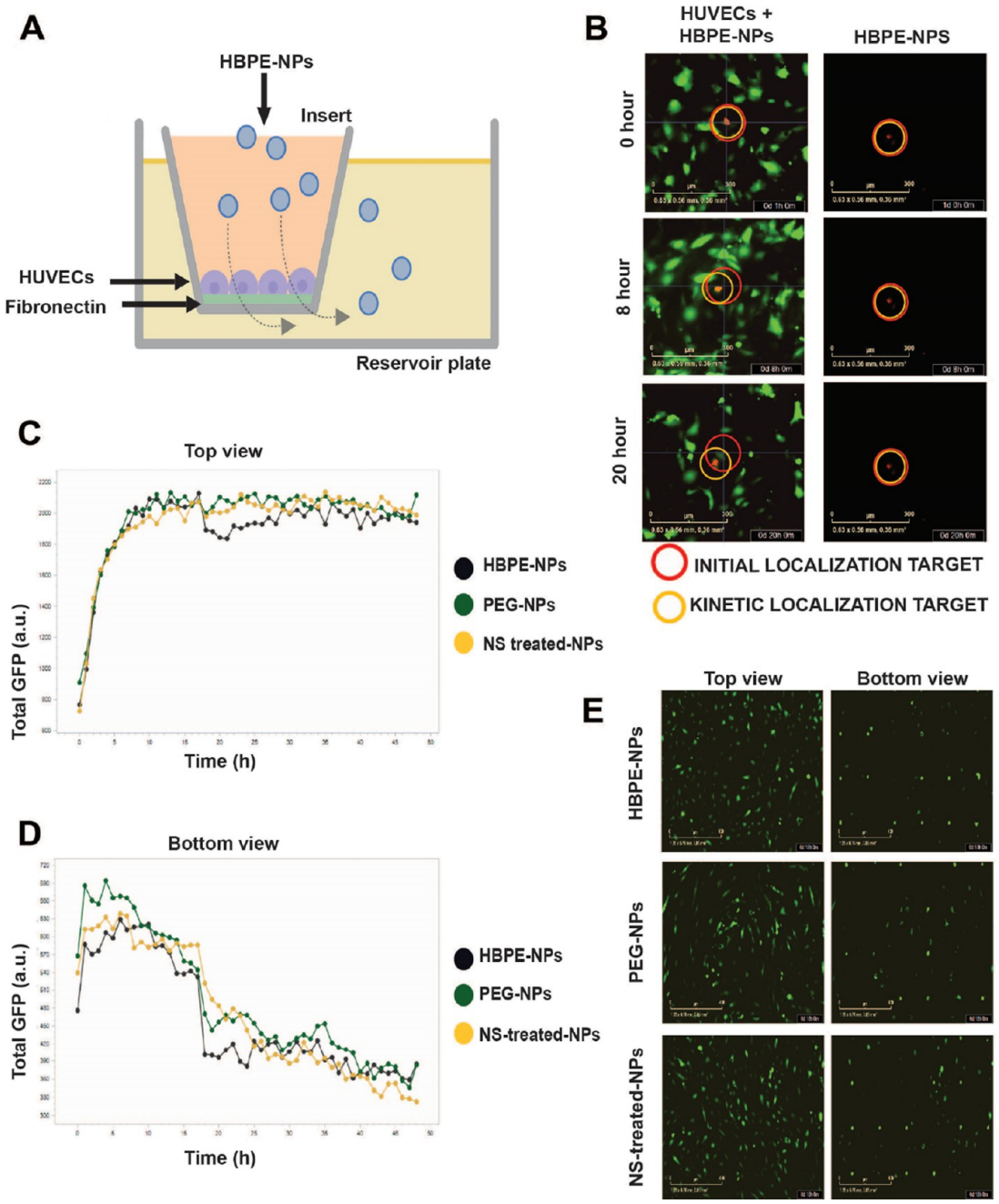

Figure 5. NS-treated HBPE-NPs do not promote endothelial cell migration. (A) Schematic for the CTEM protocol using the IncuCyte live-cell analysis system. (B) HUVECs (Cyto-Light Green) were plated at 80% confluency and treated with DiI-encapsulated HBPE-NPs. Imaging was performed at 0.5 h intervals for 24 h detecting the green fluorescent (cells) and red fluorescent (nanoparticles) channels. Time course videos were made using the IncuCyte's chemotaxis software and select videographs analyzed for movement of red fluorescent particles. Red circles show the initial nanoparticle target site at time 0 and yellow circles show the location of the nanoparticle target after 20 h. (C, D) Total green fluorescence graphs of HUVEC cells (Cyto-Light Green) treated with DiI-encapsulated COOH-HBPE-NPs (COOH-NPs), PEG-HBPE-NPs (PEG-NPs), and NS-treated HBPE-NPs are shown. Graphs track the migration of HUVEC cells above (C) or below (D) the insert through 48 h (1 h increments). (E) Representative top and bottom views of insert for fluorescent HUVEC cells at 18 h posttreatment with PEG-NPs, HBPE-NPs, or HBPE-NPs (NS).

treated HBPE-NPs not incubated with the anti-IgG antibody. Since the diameters of NS-treated HBPE-NPs increased upon the anti-IgG antibody addition, but not the untreated COOH-HBPE-NPs (Table 2), it is suggestive that HBPE-NPs formed a protein corona when exposed to NS. To confirm, we determined that HBPE-NPs could concentrate serum proteins by analyzing the protein content of HBPE-NPs treated with NS at a 20:1 or 5:1 volume-to-volume ratio by gel electrophoresis and staining with Coomassie Blue (Figure S2).

After DLS data confirmed the capacity of HBPE-NPs to form a protein corona with NS, we visualized corona formation by TEM. NS-treated HBPE-NPs resulted in observable nanoparticle agglomeration that was not seen with NS alone (Figure 3A), confirming the presence of NS-treated HBPE-NPs. Our data suggests that HBPE-NPs can form a protein

https://dx.doi.org/10.1021/acsomega.0c05998
ACS Omega 2021, 6, 5591−5606

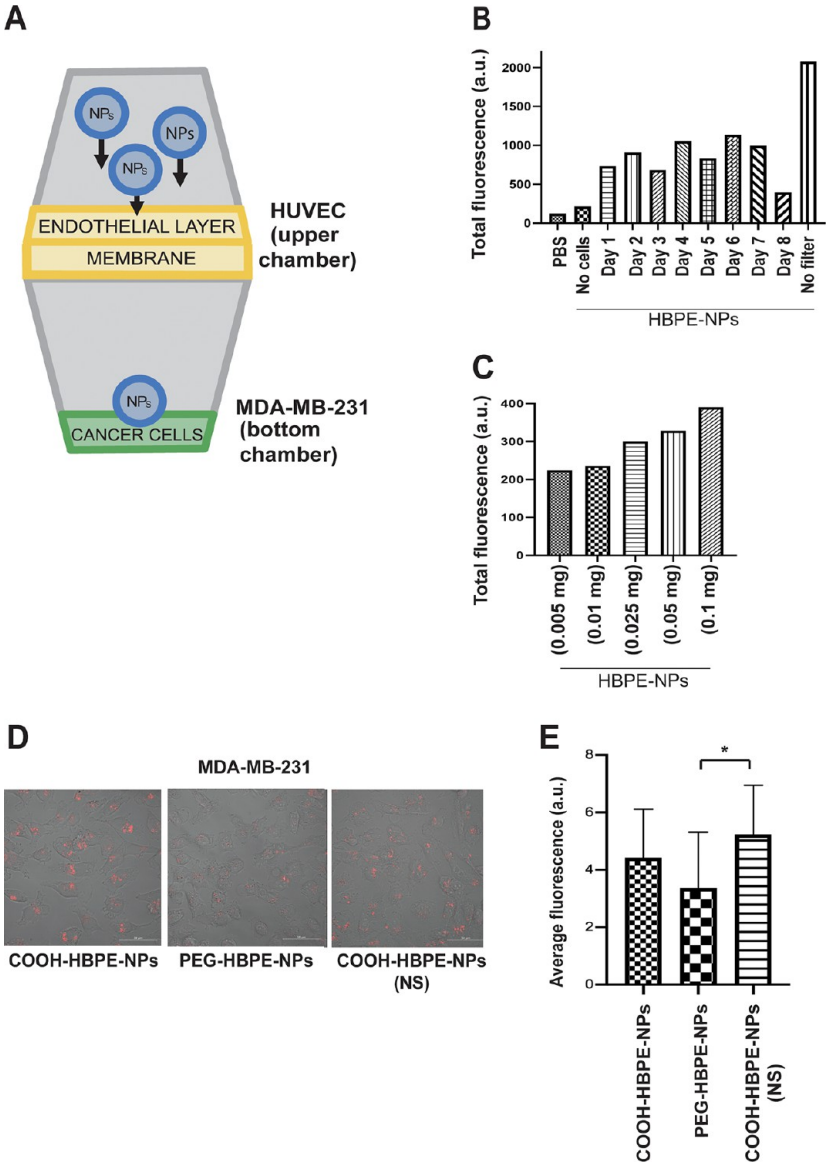

Figure 6. NS-treated HBPE-NPs are taken up by cancer cells after passage through the endothelial layer. (A) Schematic for a transwell plate system consisting of a HUVEC-seeded insert and an MDA-MB-231-seeded bottom chamber. (B) Bar graph depicts optimization of HUVEC density. HUVECs were seeded at 60% confluency and proliferated through 8 days. At each timepoint, COOH-HBPE-NPs loaded with DiI were added to the top chamber and media from the bottom chamber collected for assessment of fluorescence using the Cytation 5 plate reader. (C) Bar graph depicts optimization of the COOH-HBPE-NP treatment dose. HUVECs were seeded as in (B) and DiI-loaded COOH-HBPE-NPs added at increasing concentrations. After 24 h, fluid from the bottom chamber was collected and total fluorescence determined as above. (D) Representative confocal microscopy images (single cell plane) of the bottom chamber containing MDA-MB-231 cells. HUVECs were treated with DiI-encapsulated COOH-HBPE-NPs, PEG-HBPE-NPs, and NS-treated COOH-HBPE-NPs. Images of nanoparticle uptake by MDA-MB-231 cells were acquired 24 h posttreatment. Scale bar represents 50 μm. Images were taken with a Zeiss LSM 710 microscope at 40× magnification. (E) Bar graph of digital images acquired from (D). Average DiI fluorescence per cell is shown (n = 100 cells). Images were taken by a Cytation 5 cell imaging multi-mode reader (see Figure S4 for representative images). Data represents mean ± standard deviation. *p-value <0.0001 relative to PEG-HBPE-NPs. Representative data from three replicates is shown.

corona that is based on the HBPE polymer chemical structure. To ensure that cellular uptake would not be influenced by any adverse effects of NS-treated HBPE-NPs on MDA-MB-231, HUVEC, or THP-1 cells, an MTT (3-[4,5-dimethylthiazole-2-yl]-2,5-diphenyltetrazolium bromide) viability assay was performed (Figure 3B). Treatment of cells with NS-coated HBPE-NPs after 24 h showed no toxic effects, and viability was comparable to that of vehicle control (no NPs) or untreated HBPE-NPs. Note that these and subsequent experiments were performed in standard tissue culture media that contains 10% fetal bovine serum (FBS). Hence, untreated HBPE-NPs were included in all experiments as a control for the nonspecific adsorption of proteins from FBS and to demonstrate that the pretreatment of HBPE-NPs with NS, much like PEGylation, alters coronae formation, even in FBS-containing media.

Direct Uptake of NS-Treated HBPE-NPs by Monocytic, Endothelial, and Cancer Cells. Once HBPE-NPs were confirmed to form a protein corona using DLS and TEM, *in vitro* studies were performed to evaluate whether the protein corona affected the ability of HBPE-NPs to be taken up by cells. Human-derived cell lines MDA-MB-231, HUVEC, and THP-1 were used, representing TNBC, endothelial, and

https://dx.doi.org/10.1021/acsomega.0c05998
ACS Omega 2021, 6, 5591−5606

monocytic cells, respectively. NS-coated HBPE-NPs loaded with DiI were incubated with MDA-MB-231, HUVEC, and THP-1 cells for 24 h. PEGylated, DiI-loaded HBPE-NPs were included as a comparison to a standard in the field, and untreated DiI-loaded HBPE-NPs used as a control for non-specific uptake of media-related proteins as indicated above. Note that nanoparticle preparations all had equivalent loadings of DiI dye (Figure S1A). To visualize internalization of DiI loaded HBPE-NPs by individual cells, laser confocal scanning microscopy was performed. To quantitate total fluorescence in a microscopic field of cells, digital microscopy coupled to a plate reader was used. Together, these two methods provide qualitative and quantitative evaluation of the nanoparticle uptake by cells. Hence, images were acquired by confocal (Figure 4A) and digital (Figure S3) microscopy to show mid-cell plane and total fluorescence, respectively. Fluorescence quantification was performed on digital images (Figure S3) by averaging pixel intensity per cell. In MDA-MB-231 cells (Figure 4A,B), NS-treated-HBPE-NPs exhibited a significantly higher uptake ($p < 0.0001$) compared to PEG-HBPE-NPs. With THP-1 cells and HUVECs, comparable uptake was noted between NS-treated and PEG-HBPE-NPs (Figure 4A,C,D), suggesting that NS-treatment did not enhance immune cell recognition or alter endothelial uptake. From these results, we surmise that NS contains proteins not found in PEGylated particles that are advantageous for the delivery of HBPE-NPs to cancer cells while evading monocyte uptake. The non-specific adsorption of media-derived proteins by untreated COOH-HBPE-NPs served as a positive control for uptake of particles by breast cancer cells[22] and represented optimal outcomes achievable under *in vitro* cell culture. It is important to note that under *in vivo* conditions such untreated particles may be rapidly cleared and are not relevant in animal models; hence, these are only used as controls for the *in vitro* studies.

Interaction of NS-Treated HBPE-NPs with Cancer Cells in an Endothelial-Based Transwell System. The *in vivo* administration of drug-loaded HBPE-NPs may require that particles transit in the bloodstream and move through the vascular endothelium to reach tumor cells.[2] Hence, it is important to determine whether NS-treated HBPE-NPs that transit through endothelial cells can subsequently penetrate tumor cells. To investigate this, we first used the chemotaxis transendothelial migration (CTEM) protocol associated with the IncuCyte live-cell analysis system to study the interaction of HBPE-NPs with HUVECs. The CTEM is a two-part system in which an insert is treated with fibronectin, and green fluorescent HUVECs (for tracking) are seeded up to 9000 cells/well. The insert is placed inside of a reservoir plate with media (schematic, Figure 5A) and loaded into the IncuCyte instrument, which scans (at 10× magnification) the top and bottom of the insert membrane over a two-day period at hourly intervals. Our initial optimization of HUVEC seeding density showed that, over a 20 h period, dye-loaded HBPE-NPs (red signal) did not move from the insert plate unless HUVECs (green signal) were present; hence, free HBPE-NPs stay in the insert, likely trapped in the fibronectin layer, and move into the reservoir plate when facilitated by interaction with HUVECs (Figure 5B). These results suggest that complete confluency of the HUVEC layer may not be needed to prevent free HBPE-NPs from entering the reservoir plate; this is further assessed in subsequent figures. To determine whether HBPE-NPs did not induce the migration of HUVECs, which could promote angiogenesis and tumor growth, DiI-loaded NS-treated HBPE-NPs and controls, PEG- and COOH-HBPE-NPs, were added to the insert containing HUVECs (at ∼80% confluency). Cells were imaged, above and below the insert, at 0.5 or 1 h intervals for 24 or 48 h, accordingly, for detection of green fluorescence. Total fluorescence in the green channel (above and below insert pores) was quantified (Figure 5C,D). Since total green fluorescence (indicative of HUVECs presence) for all nanoparticle treatments was comparable above the pore layer and consistently decreased over time below the pores, this implied a similar rate of migration irrespective of nanoparticle presence. Hence, the treatment of HUVECs with HBPE-NPs (NS-treated or controls) did not enhance migration in a manner that could promote subsequent tumor growth. Representative images of green fluorescent HUVECs present above and below pores of the insert are additionally shown (Figure 5D).

We next evaluated cancer cell uptake of NS-treated HBPE-NPs utilizing a modified transwell system. The transwell system consists of an upper chamber containing a layer of HUVEC cells (initially plated at ∼80% confluency), a membrane that separates the chambers, and a lower chamber in which MDA-MB-231 cells are plated (schematic, Figure 6A). In this way, aspects of the distribution behavior of HBPE-NPs moving through an endothelial layer into tumor tissue could in part be simulated *in vitro*. While this system does not replicate the fluid dynamics of blood, it enables the evaluation of the cellular interactions involved in transendothelial movement and cancer cell uptake of particles. To confirm that HUVECs were needed for the movement of HBPE-NPs between chambers, HUVECs were seeded in equal numbers per well and allowed to proliferate up to 8 days. HPBE-NPs were introduced into the top chamber from each (day 1 to 8), and fluid was collected from the bottom chamber for detection of fluorescent particles by digital imaging. Controls included phosphate-buffered saline (PBS), HBPE-NPs alone (negative control), and HBPE-NPs directly introduced into the bottom chamber (positive control). Few of the HBPE-NPs introduced into the upper chamber were detected in the lower chamber in the absence of HUVECS, which confirmed results observed with the CTEM protocol (Figure 5B). In the presence of HUVECs, 3−5-fold higher amounts of fluorescent HBPE-NPs were detected in the bottom chamber, a result that was independent of cell proliferation (Figure 6B).

After confirming that, in the absence of HUVECs, HBPE-NPs did not move effectively through transwell pores and determining that HUVECs were sufficiently confluent by 24 h after seeding to promote the movement of NPs into the bottom chamber; these conditions were used for subsequent transwell experiments. Note that post-day 8, HUVECs began to die under these culture conditions, further supporting that live HUVECs were needed for the movement HBPE-NPs between chambers. We next determined the optimal nanoparticle dose to detect the movement of HBPE-NPs through a layer of HUVECs. A dose range of 0.005, 0.01, 0.025, 0.05, and 0.1 mg (based on HBPE polymer concentration) was used to treat HUVECs for 24 h. An amount of 0.1 mg served as a reference dose that was used in the previous *in vitro* experiments. Following treatment, NPs were collected in the bottom chamber, and DiI dye total fluorescence was measured. We observed that an increase in bottom chamber fluorescence was directly proportional to the nanoparticle treatment dose listed above (Figure 6C). After determining a limit of detection

https://dx.doi.org/10.1021/acsomega.0c05998
ACS Omega 2021, 6, 5591−5606

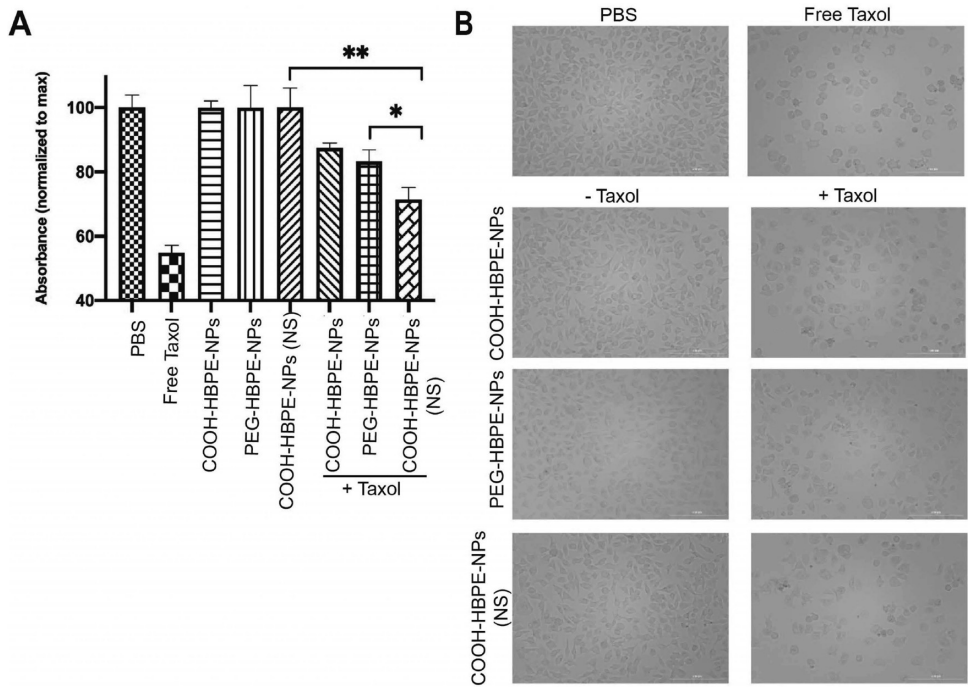

Figure 7. Increased killing of TNBC cells by taxol-loaded NS-HBPE-NPs. (A) MDA-MB-231 cells were treated with free taxol (50 nM or 43 μg), and COOH-HBPE-NPs, PEG-HBPE-NPs, and NS-treated COOH-HBPE-NPs with or without taxol (0.01 mg polymer; 0.5−0.6 μg taxol) for 24 h. Cell viability was assessed using an MTT assay. Data in graph displays mean ± standard deviation (n = 3). *p = 0.0283, **p = 0.0020. (B) Representative images of MDA-MB-231 cells treated as in (A) using the Cytation 5 cell imaging multi-mode reader.

of approximately 0.005 mg of the nanoparticle, a 0.1 mg nanoparticle dose was chosen for subsequent transwell studies.

After optimizing the transwell experimental protocol, we determined whether NS-treated HBPE-NPs that initially interacted with endothelial cells could still be taken up by cancer cells. Controls included PEG-HBPE-NPs as a standard for comparison and untreated HBPE-NPs to capture the optimal uptake in culture media. After HBPE-NPs were incubated with HUVECs (upper chamber) for 24 h, uptake of particles by individual MDA-MB-231 cells (bottom chamber) was visualized by confocal microscopy (Figure 6D) and total fluorescence in a microscopic field of cells quantitated by digital microscopy coupled to a plate reader (Figure S4 and Figure 6E). A statistically significant increase in the uptake of NS-treated HBPE-NPs by TNBC cells was observed as compared to PEGylated HBPE-NPs. These results suggest that the protein coronae formed on HBPE-NPs after treatment with NS still facilitated uptake by cancer cells, even after a prior interaction with the endothelial cell monolayer.

Drug Delivery to Cancer Cells Is Enhanced by NS-Treated HBPE-NPs. To evaluate the capacity of the NS-treated HBPE-NPs to deliver drug cargo to breast cancer cells, we encapsulated HBPE-NPs with taxol and determined that NPs were equivalently loaded with drug cargo (Figure S1B; ∼0.5−0.6 μg taxol loaded per 0.01 mg HBPE polymer). We established the IC50 dose of free taxol to be ∼50 nM (43 μg). We then compared the capacity of NS-treated HBPE-NPs to deliver taxol to breast cancer cells as compared to PEGylated HBPE-NPs, using a 0.01 mg dose of HBPE-NPs to observe relative differences in viability. All taxol-loaded nanoparticle preparations caused increased death of cancer cells as compared to drug-free HBPE-NPs (Figure 7A,B), showing that HBPE-NPs could be effectively loaded with drug cargo. Based on our previous uptake data (Figures 4B and 6E), we anticipated that NS-treated HBPE-NPs would more efficiently deliver taxol to cancer cells. This was observed after 24 h of treatment of MDA-MB-231 cells with taxol-loaded NS-treated HBPE-NPs. A statistically significant decrease in viability was noted as compared to taxol-loaded, PEGylated HBPE-NPs, and taxol-loaded COOH-HBPE-NPs (Figure 7A). This was confirmed microscopically using digital imaging (Figure 7B). Moreover, HBPE-NPs achieved taxol-mediated killing at doses of taxol that were significantly than free drug.

DISCUSSION

The formation of the protein corona on polymeric NPs is a critical parameter that affects the performance of these particles when loaded with clinically relevant drugs like taxol. Characterization of this protein layer is thus important when developing new nanomedicines. While more is known on coronal formation using metallic NPs, much less is known about the protein corona that forms with polymeric NPs,[41,42] and no information is available on the proteins that associate with NPs made using the malonate-based HBPE polymer described herein. This is the first study revealing that HBPE-NPs can enrich for select sera proteins that enhance the uptake of particles by cancer cells over PEGylated HBPE-NPs, even after an initial interaction with an endothelial layer, and deliver cytotoxic doses of a hydrophobic drug like taxol. Hence, HBPE-NPs are a promising platform for new discovery that advances the generation of biomimetic NPs.

Taxanes (e.g., paclitaxel, docetaxel, cabazitaxel) are a widely used class of antimitotic drugs for cancer treatment, but their application is characterized by severe off-target effects that include hypersensitivity reactions, peripheral neuropathy, and other toxicities. As a result, in some patients, the beneficial use of taxanes is limited. Nanocarriers solve this problem. An example is BIND-014, a polymeric nanoparticle loaded with

https://dx.doi.org/10.1021/acsomega.0c05998
ACS Omega 2021, 6, 5591−5606

docetaxel that targets tumors through PSMA.[43] In clinical trials, the toxicity profile of BIND-014 was found to be similar to free docetaxel and showed patient benefit in prostate cancer.[44] Other drug delivery systems for taxanes include liposomes that are PEGylated[45] to generate stealth nanocarriers. However, such particles could be subject to accelerated blood clearance and have issues with batch-to-batch reproducibility. Polymeric micelles encapsulating taxanes have also reached clinical trials (NANT-008[46] and NK105[47]) and display increased tumor accumulation in preclinical studies and positive outcomes in clinical trials with varying degrees of adverse effects including hypersensitivity. Of the polymeric NPs, poly(lactic-*co*-glycoic acid) (PLGA) is most commonly used but other natural (e.g., albumin) or synthetic polymers are also employed. Nab-paclitaxel (Abraxane) is the only FDA-approved albumin-based nanoparticle that delivers paclitaxel likely via albumen-driven transcytosis (e.g., transcellular transport).[48] Despite preclinical and clinical trial successes, clinical evidence that use of NPs leads to increased tumor accumulation of taxanes is lacking. Part of the reason could be the need for a better understanding of the interface between NPs and the surrounding biofluids and how this affects biodistribution and cancer cell uptake. We show that NPs, formed using HBPE, can have different cellular uptake outcomes, based on whether a particle is PEGylated or pretreated with NS, and this impacts the delivery and subsequent cytotoxicity of taxol.

Being able to anticipate or predict how the formation of a protein corona on NPs will affect *in vivo* biological processing is a pressing need. In general, the major proteins found in the protein corona formed on NPs exposed to sera can either promote clearance by the RES (e.g., opsonins like complement), which is reduced by PEGylation, or have less affinity for cell surfaces and improve blood circulation (e.g., dysopsonins like serum albumin). Nano-liquid chromatography−tandem mass spectrometry revealed that the adsorbed proteins from normal human plasma on PLGA-NPs changed based on the size, charge, and composition of particles and showed positive and negative correlations between dysopsonins and opsonins. Common and unique proteins were identified such as albumin and immunoglobulins, respectively.[49] HBPE-NPs in our study were also able to enrich for common proteins and unique immunoglobulins, as shown by gel electrophoresis and DLS experiments with anti-IgG antibodies, suggestive of comparable results. To more directly assess the effectiveness of a protein corona derived from healthy sera, transferrin (Tf)-modified polystyrene NPs were treated with the plasma from normal individuals as compared to lung cancer patients and uptake by A549 lung cancer cells determined. Tf-NPs coated with normal sera were more effectively internalized by lung cancer cells. The negative effect of exposure to disease-derived biofluid was reversed by precoating these Tf-NPs with sera from healthy mice.[42] Similarly, we found that HBPE-NPs pretreated with NS from mice improved the delivery of taxol-loaded HBPE-NPs compared to PEGylated HBPE-NPs. Characterizing the proteome enriched on Tf-NPs exposed to normal plasma compared to lung cancer patient plasma revealed differences in major proteins: less albumin and more complement proteins in lung cancer plasma-derived NPs and higher levels of alpha-2 macroglobulin (A2M) in normal plasma-derived NPs.[42] These results, together with our findings, suggest that protein coronas derived from healthy biofluids could improve the clinical applications of nanomedicines.

Further studies of the protein coronas of NPs are needed to investigate the dynamics of the nanoparticle proteome and fully develop new technologies to improve cancer drug delivery. One challenge is accurately assessing the composition of protein coronae given that the configuration of the nanoparticle-host serum interface may be a complex arrangement of different macromolecules or aggregations.[50] This could lead to over or underestimation of the actual protein content adsorbed by NPs. Studies showed that composition of proteins bound to NPs may depend on the nanoparticle to sera concentration.[51] Plasma variance among individuals is another factor that influences the interaction of NPs and could lead to the generation of personalized biomolecular coronas to control nanoparticle targeting.[52] To this end, the physio-chemistry of HBPE-NPs could lead to the discovery of novel sera-derived factors as indicated by our findings. This was the case with NPs formed using other polymers like PLGA or polycaprolactone (PCL) in which unique nano-proteome fingerprints were detected depending on the polymer used.[53] PLGA-NPs bound human sera proteins with lower affinity compared to PCL-NPs, which adsorbed distinct proteins. The concept that NPs can be functionalized with natural materials, such as by protein adsorption,[54] is emerging as a viable approach for improving bioavailability. Moreover, identifying coronal proteins could help trace the transport pathways of particles through epithelial and endothelial layers and help reveal mechanisms of transcytosis.[55] Using particles like HBPE-NPs to enrich for and discover both the high and low abundance proteins[27] from sera or other relevant biofluids, as demonstrated in our data, is an important step to advance novel precoated NPs for therapeutic and diagnostic uses in the treatment and detection of cancer.

CONCLUSIONS

Utilizing NPs to improve drug delivery to tumors is a promising approach for enhancing the efficacy of cancer therapies. To this end, the capacity of NPs to selectively adsorb proteins from biofluids, like normal mouse sera, can be used for discovery of novel factors to functionalize nanodrug carriers for testing in preclinical cancer studies. We investigated whether NPs formed using the HBPE polymer could adsorb components from NS that would endow the particles with cancer cell uptake capacity that was as good, if not better, than a standard antifouling approach like PEGylation. Using a TNBC cell line, as well as endothelial and monocytic cells, we found that NS-treatment increased the uptake of HBPE-NPs by cancer cells, as compared to PEG-HBPE-NPs, while not enhancing monocyte uptake. Hence, the coating on HBPE-NPs provided by treatment with NS could facilitate the internalization particles by cancer cells without augmenting immune clearance. NS-treated HBPE-NPs were inherently nontoxic and did not stimulate the migration of endothelial cells. The NS-derived corona formed on HBPE-NPs improved cancer cell uptake, even after an initial interaction with endothelial cells. Loading NS-treated HBPE-NPs with taxol revealed that these particles could efficiently deliver drug cargo to cancer cells, as compared PEGylated particles. These findings support the further investigation of sera-derived components enriched by HBPE-NPs to generate the next generation of biomimetic nanomedicines.

https://dx.doi.org/10.1021/acsomega.0c05998
ACS Omega 2021, 6, 5591−5606

MATERIAL AND METHODS

Materials. For nanoparticle synthesis and preparation, 2-(*N*-morpholino)ethanesulfonic acid (MES) 5× buffer (pH 7.4) was purchased from Alfa Aesar (Haverhill, MA, USA). Acetone, dimethyl sulfoxide (DMSO), ethyl acetate, hydrochloric acid (HCl), isopropanol, methanol, petroleum ether, sodium sulfate (Na_2SO_4), and other chemicals were obtained from Fisher Scientific (Waltham, MA, USA). DiI dye and DiR dye were purchased from Life technologies (Carlsbad, CA, USA). 4-Bromobutyl acetate (BBA), acetonitrile, diethyl malonate (DEM), 1-ethyl-3-(3-dimethylaminopropyl)-carbodiimide (EDC), iodine crystals, *N*-hydroxysuccinimide (NHS), poly(ethylene glycol) 2-aminoethyl ether acetic acid 10,000 MW, potassium carbonate (K_2CO_3), *p*-toluenesulfonic acid (PTSA), silicone oil, sodium hydroxide (NaOH), and terephthalic acid were obtained from MilliporeSigma (Burlington, MA, USA). Purified deionized water was acquired through a Milli-Q purification system from MilliporeSigma.

For nanoparticle characterization, methyl sulfoxide-d_6 (DMSO-d_6) was purchased from Acros organics (Geel, Belgium) and anti-mouse IgG (Fab-specific) goat antibody was purchased from MilliporeSigma.

For cell studies, Ham's F-12K (Kaighn's) medium, HUVEC (CRL-1730) cells, THP1 (TIB-202), and MDA-MB-231 (HTB-26) cells were obtained from ATCC (Manassas, VA, USA). Neutral buffered formalin (10%) was obtained from Azer Scientific Inc. (Morgantown, PA, USA). Dulbecco's modified Eagle medium (DMEM), endothelial cell growth supplement (ECGS), L-glutamine, PBS, penicillin−streptomycin solution (10,000 U/mL), and 0.25% trypsin (0.1% EDTA in HBSS) were purchased from Corning (Corning, NY, USA). FBS was obtained from Gemini Bio-Products (Sacramento, CA, USA). Heparin sodium salt from porcine intestinal mucosa was purchased from MilliporeSigma. 3-(4,5-Dimethylthiazolyl-2)-2,5-diphenyl tetrazolium bromide (MTT) was obtained from MP Biomedicals (Santa Ana, CA, USA). 4′,6-Diamidino-2-phenylindole (DAPI), 10% neutral buffered formalin, and fibronectin bovine protein were purchased from ThermoFisher Scientific (Waltham, MA, USA). Paclitaxel (taxol equivalent) was obtained Thermofisher Scientific.

For gel electrophoresis, Mini-PROTEAN TGX polyacrylamide gels and Precision Plus protein dual-color standard protein ladder were purchased from Bio-Rad Laboratories (Hercules, CA, USA). β-Mercaptoethanol was obtained from Millipore Sigma. Coomassie Brilliant Blue was purchased from ThermoFisher Scientific.

Compound 1: Synthesis of 2-(4-Acetoxy-butyl)-malonic Acid Diethyl Ester. To a 2000 mL round bottom flask containing 1000 mL of acetonitrile were added sequentially K_2CO_3 (155.72 g), DEM (45.13 g), and BBA (50 g) at molar equivalents of 1, 1.1, and 1, respectively, and mixed under stirring for 10 min at room temperature. The solution was refluxed for 36 h to synthesize compound **1**. A 500 mL separatory funnel was used to extract excess DEM and compound **1** in ethyl acetate and discard K_2CO_3 and acetonitrile through deionized water. Excess DEM and compound **1** were filtered through Na_2SO_4 to remove water carryover. Rotary evaporation under vacuum was used to remove ethyl acetate at 70 °C. Vacuum distillation was employed to remove excess DEM at 90 °C. Thin-layer chromatography (TLC) silica gel plates (MilliporeSigma) in a developing chamber solution of 10% ethyl acetate in petroleum ether were used with an iodine crystal chamber to verify compound **1** purification. NMR was performed to confirm compound **1** synthesis.

Compound 2: Synthesis of 2-(4-Hydroxy butyl)-malonic Acid. Purified compound **1** (5 g) was added to 200 mL of methanol and 110 mL of NaOH (2 M) in a 250 mL round bottom flask under stirring for 10 min at room temperature. The mixture was refluxed for 18 h. Subsequently, 200 mL of HCl (1 M) was added drop wise, 10 mL at a time, under stirring, to the refluxed solution until an acidic solution (pH 1) was achieved. The solution underwent vacuum distillation for 18 h at 90 °C to synthesize compound **2**. To the distilled solution was added 35 mL of isopropanol, followed by centrifuging at 3000×*g* for 10 min. The precipitate, containing sodium chloride (NaCl), was discarded. The supernatant was extracted and put through rotary evaporation under vacuum to purify compound **2** from isopropanol and methanol. TLC was performed to verify compound **2** purification. NMR was carried out to confirm compound **2** synthesis.

Compound 3: Synthesis of HBPE Polymer. Compound **2** (monomer, 120 mg) was diluted to 90 mg/mL in DMSO and subsequently aspirated through a 3 mL BD Luer-Lok syringe (Fisher Scientific) using an 18-gauge syringe needle (Fisher Scientific). The syringe was placed vertically on a NE-300 syringe pump (New Era Pump Systems Inc., Farmingdale, NY, USA) and positioned within a rubber-capped neck of a 50 mL double-necked round-bottom flask. To the 50 mL double-necked flask, 4.75 mL of DMSO and 250 μL of PTSA at 5 mg/mL were added prior to syringe insertion. The monomer-to-PTSA molar ratio was 100:1. The syringe pump was set to dispense the monomer solution at a 0.1 mL per hour rate. The reaction was run for 15 h at 130 °C under a nitrogen atmosphere. The polymer (compound **3**) was dissolved in DMSO at 20 mg/mL. DMSO was removed through lyophilization to dissolve polymer in DMSO-d_6 for NMR preparation. NMR was used to verify the polymer synthesis. The procedure for seed-based HBPE polymer synthesis was adopted from the HBPE polymer synthesis method above with some modifications. All synthesis steps were identical for seed-based and nonseed-based HBPE polymers with the following exceptions. To the 50 mL double-necked flask, 4.75 mL of DMSO, 250 μL of PTSA at 5 mg/mL, and 500 μL of terephthalic acid at 12 mg/mL were added prior to syringe insertion. The monomer to PTSA molar ratio was 100:1. The monomer-to-terephthalic acid molar ratio was 20:1.

Nanoparticle Synthesis, Drug/Dye Encapsulation, and PEG Functionalization. HBPE-NPs were formed and encapsulated with dye or drug as follows. For dye-loaded NPs, 0.001 mg of DiI or DiR dye in 100 μL of DMSO (HBPE-DiI/DiR NPs) was added to 10 mg of HBPE polymer. For drug-loaded NPs, 2 mg of taxol was added to 10 mg of HBPE polymer. The mixture was then added dropwise, 10 μL at a time, to 4 mL of deionized water under vortex at 2000 rpm. For PEG functionalization, EDC (1.5 mg), NHS (0.5 mg), and PEG (1 mg) were weighed. Subsequently, EDC and NHS were dissolved in 100 μL of 1× MES buffer, while PEG was dissolved in 100 μL of deionized water. EDC, NHS, and PEG solutions were added individually to COOH-HBPE-DiI/DiR-NPs and incubated for 10 s, 3 min, and 4 h, respectively, using a Rotamix (ATR biotech, Laurel, MD, USA). A Sephadex G-25 PD-10 desalting column (GE Lifesciences, Chicago, IL, USA) was used to remove excess dye, drugs, EDC, NHS, or PEG.

https://dx.doi.org/10.1021/acsomega.0c05998
ACS Omega 2021, 6, 5591−5606

NPs were then filtered through a 0.22 μm polyethersulfone (PES) membrane (MilliporeSigma). Afterward, NPs were concentrated to 10 mg/mL, using an Amicon Ultra-4 centrifugal filter unit (MilliporeSigma) at 1600×*g* for 15 min cycles. All encapsulation and functionalization procedures were performed at room temperature.

To verify uniform dye and taxol encapsulation in NPs, fluorescence and absorbance quantifications for DiI and taxol, respectively, were performed. To assess DiI encapsulation, a calibration curve was established with serial dilutions of DiI (Figure S1A). Then, 10 μg of COOH-or PEGylated DiI-encapsulated NPs was dispensed in an HCl-acidified PBS solution (pH = 4) and incubated for 6 h at room temperature to release encapsulated DiI upon HBPE polymer ester hydrolysis. DiI fluorescence was measured with a Cytation 5 cell imaging multi-mode reader at 531 nm excitation and 593 nm emission wavelengths. To assess taxol encapsulation, a calibration curve was established with serial dilutions of taxol (Figure S1B). Then, 10 μg of COOH or PEGylated taxol-encapsulated NPs was incubated in an HCl-acidified PBS as above to release taxol and absorbance (UV/Vis) was read at a 250 nm wavelength using a Beckman Coulter DU 800 spectrophotometer (Brea, CA, USA).[56] Trendline equations of the serial dilutions for estimation of encapsulated DiI or taxol concentration in the NPs were performed, except the trendline's *y*-axis value being absorbance for taxol and fluorescence for DiI.

HBPE Polymer and Nanoparticle Characterization. *Nuclear Magnetic Resonance (NMR).* NMR spectra were recorded on Bruker Avance III 400 MHz and Varian VNMRS 500 MHz spectrometers with solvent signal used as an internal reference. Samples in DMSO-d_6 were calibrated with the solvent, and samples in D_2O calibrated with the CH_3 peak of residual undeuterated acetic acid. The following abbreviations were used to explain the multiplicities: t = triplet, q = quartet, quint = quintet, br = broad singlet or broad multiplet.

HBPE monomer, ^{1}H NMR (400 MHz, D_2O, δ ppm) δ = 3.47 (t, J = 6.6 Hz, 2H), 3.07 (t, J = 7.2 Hz, 1H), 1.69 (q, J = 7.7 Hz, 2H), 1.44 (quint, J = 7.2 Hz, 2H), 1.20 (quint, J = 7.8 Hz, 2H).

HBPE polymer, ^{1}H NMR (500 MHz, DMSO-d_6, δ ppm) δ = 4.87 (br, 1H), 3.60 (br, 2H), 3.34 (br, 1H), 1.70 (br, 2H), 1.52 (br, 2H), 1.24 (br, 2H).

Transmission Electron Microscopy. Uncoated or serum-coated NPs (0.05 mg) were dispensed onto a 400-mesh copper grid (Ted Pella Inc., Redding, CA, USA). Excess solution was removed with a Kimwipe (Kimberly-Clarke, Iriving, TX, USA) and left to air-dry overnight at room temperature. Grids were imaged with a JEOL TEM-1011 (JEOL Ltd., Akishima, TYO, Japan) microscope at 100 kV and 6000 magnification.

DLS Analysis and IgG Detection. NPs (0.1 mg) were dispersed in 800 μL of deionized water in a folded capillary Zetacell (Malvern Panalytical, Worcestershire, U.K.). Nanoparticle hydrodynamic diameter and zeta potential were then measured with a Malvern Zetasizer ZS90 (Malvern Panalytical) instrument at room temperature. Regarding serum- and antibody-related experiments, a 20:1 volumetric ratio of 0.1 mg of NPs to mouse serum, or 2 mg/mL of IgG antibody, was used. NPs were incubated with either serum alone, or serum and subsequently antibody, for 15 min each. Incubations were done under gentle agitation at room temperature. All diameter and zeta potential values are averages of three replicates.

Cell Culture. MDA-MB-231 TNBC cells were cultured in DMEM supplemented with 10% FBS, 2 mM L-glutamine, and 1× penicillin−streptomycin. HUVEC endothelial cells (Cytolight Green) (Essen BioScience) were cultured in F-12K media supplemented with 10% FBS, 2 mM L-glutamine, 1× penicillin−streptomycin, 56 mg of heparin sodium salt, and 15 mg of ECGS. THP-1 cells were cultured in an RPMI1640 medium supplemented with 2mercaptoethanol 0.05 mM, 10% FBS, 2 mM L-glutamine, and 1× penicillin−streptomycin. All cell lines were limited to a low number of passages and incubated in 5% CO_2 at 37 °C.

MTT Viability Assay. For cell viability assays, either deionized water (vehicle) or 0.1 mg of HBPE-NPs was used. Treatments were dispensed in 96-well culture plates, seeded with 0.5 × 10^4 MDA-MB-231, HUVEC, or THP-1 cells at 60% confluency. Culture plates contained 100 μL of media per well. After 24 h treatment, 0.05 mg of the MTT reagent was dispensed in each treated well and incubated for 4 h in 5% CO_2 at 37 °C. Media was then removed and replaced with 100 μL of DMSO. Culture plates were shaken for 15 min at 800 rpm. Absorbance was measured at 570 nm using a Cytation 5 cell imaging multi-mode reader (BioTek, Winooski, VT, USA). Deionized water served as a negative control.

Cell Uptake Studies. 0.5 × 10^4 MDA-MB-231, HUVEC or THP-1 cells were seeded in 96-well culture plates containing 100 μL of media per well. For precoating NPs with sera, a 20:1 volumetric ratio of 0.1 mg of NPs to NS was used. NPs were incubated with NS for 15 min. Incubations were done under gentle agitation at room temperature. Cells were grown until 60% confluency and incubated with 0.1 mg of NS-treated, COOH-HBPE-NPs, or PEG-HBPE-NPs. All NPs were loaded with DiI dye. Cells were incubated with NPs for 24 h in 5% CO_2 at 37 °C. Afterward, cells were washed with PBS, followed by fixation in 10% neutral buffered formalin for 10 min, and washed for a second time with PBS. Cells were imaged with a Zeiss LSM 710 confocal microscope (Carl Zeiss AG, Oberkochen, Germany). Analysis of intracellular fluorescence representative of particle uptake per individual cell was performed with ZEN blue software. To assess cellular uptake of fluorescent particles in a population of cells, digital imaging coupled to a fluorescent plate reader was performed with the Cytation 5 cell imaging multi-mode reader. Total fluorescence per field of cells was captured and analyzed with ZEN blue software.

Chemotactic Transendothelial Migration (CTEM) Protocol. To evaluate nanoparticle transmigration over time, an IncuCyte S3 Live-Cell Analysis System (Essen Bioscience Inc., Ann Arbor, MI, USA) was utilized. HUVECs (Cytolight Green, Essen BioScience) were grown to 80% confluency in the upper culture plate of a fibronectin-coated ClearView 96-well chemotaxis plate (Essen BioScience). PBS was dispensed in the wells of the chemotaxis plate's bottom culture plate. Cells were then treated with 0.1 mg of HBPE-NPs, PEGylated, or HBPE-NPs pretreated with NS as above. Directly after treatment, cells were imaged at 0.5 or 1 h intervals for 24 or 48 h, respectively, using a phase, green fluorescence, and red fluorescence channels. Time courses of red fluorescence total area and green fluorescence total count were quantified and graphed using IncuCyte's chemotaxis software (Essen BioScience). Images and time course videos were additionally created using this software.

Modified Transwell Assay. HUVEC cells (3 × 10^4) were seeded per well in a polycarbonate, 8 μm pore-sized, Millicell-

https://dx.doi.org/10.1021/acsomega.0c05998
ACS Omega 2021, 6, 5591−5606

24 cell culture insert plate (MilliporeSigma). Wells contained 500 μL of media, and HUVEC cells were incubated for 48 h in 5% CO_2 at 37 °C. Afterward, the HUVEC culture plate (upper chamber) was placed over a 24-well glass-bottom culture plate (lower chamber) (Cellvis, Mountain View, CA, USA), containing MDA-MB-231 cells, to create an *in vitro* transwell system. MDA-MB-231 cells (1.5×10^4) were seeded and grown to 60% confluency in 500 μL of media per well. Then, 0.1 mg of HBPE-NPs, PEGylated, or HBPE-NPs pretreated with NS as above (DiI loaded) was dispensed per well in the upper HUVEC chamber. Cells were incubated with NPs for 24 h in 5% CO_2 at 37 °C. MDA-MB-231 cells were then fixed with 10% formalin, stained with DAPI, and then imaged with a Zeiss LSM 710 confocal microscope (Carl Zeiss AG, Oberkochen, Germany). Analysis was performed with ZEN blue software. To assess total fluorescence, cells were also imaged with a Cytation 5 cell imaging multi-mode reader and analyzed with ZEN blue software.

Mouse Studies. For nanoparticle distribution studies, 8×10^5 MDA-MB-231 luciferase-expressing (Luc) cells were orthotopically injected into the mammary fat pad of a 6-week-old Fox1-nu/nu (nude) female mouse. After the mouse's tumor reached ~1000 mm^3, the mouse was injected with 1 mg of DiR loaded, PEG-HBPE-NPs through the tail vein. After 7 h post-injection, the mouse was euthanized, and its organs were harvested. Organs were imaged for DiR fluorescence using an IVIS Lumina S5 *in vivo* imaging system (PerkinElmer, Waltham, MA, USA). Fluorescence was quantified using Living Image software. For blood collection studies, C57BL/6 female mice, 2−3 months old, were used. Blood was collected through a terminal cardiac puncture and harvested in 1.5 mL Eppendorf tubes (Eppendorf, Hamburg, Germany), left to clot at room temperature for 1 h, and then centrifuged at 13,400 rpm for 5 min with an Eppendorf Minispin (Eppendorf). All animal studies were approved by and performed under the University of Central Florida Institutional Animal Care and Use Committee (IACUC) guidelines.

Statistical Analysis. Significance was determined conducting comparisons between two experimental datasets, as example, using a parametric two-tailed unpaired *T* test with Welch's correction. At a confidence level of 95%, *p*-values <0.05 were considered significant as indicated in the figure legends. Statistical analysis was performed using GraphPad Prism 8 software.

■ ASSOCIATED CONTENT

Supporting Information

The Supporting Information is available free of charge at https://pubs.acs.org/doi/10.1021/acsomega.0c05998.

Supplemental methods for assessing cargo loading of HBPE-NPs and gel electrophoresis, supplemental figure legends, and supplemental Figures S1−S4 (PDF)

■ AUTHOR INFORMATION

Corresponding Author

Annette R. Khaled − *Burnett School of Biomedical Sciences, College of Medicine, University of Central Florida, Orlando, Florida 32827, United States;* orcid.org/0000-0001-6331-9623; Phone: 14072667035; Email: annette.khaled@ucf.edu; Fax: 14072667001

Authors

Daniel Nierenberg − *Burnett School of Biomedical Sciences, College of Medicine, University of Central Florida, Orlando, Florida 32827, United States*

Orielyz Flores − *Burnett School of Biomedical Sciences, College of Medicine, University of Central Florida, Orlando, Florida 32827, United States*

David Fox − *Nanotechnology Science Center, University of Central Florida, Orlando, Florida 32826, United States; Department of Chemistry, College of Science, University of Central Florida, Orlando, Florida 32816, United States*

Yuen Yee Li Sip − *Nanotechnology Science Center, University of Central Florida, Orlando, Florida 32826, United States; Department of Materials Science and Engineering, College of Engineering and Computer Science, University of Central Florida, Orlando, Florida 32816, United States*

Caroline Finn − *Burnett School of Biomedical Sciences, College of Medicine, University of Central Florida, Orlando, Florida 32827, United States*

Heba Ghozlan − *Burnett School of Biomedical Sciences, College of Medicine, University of Central Florida, Orlando, Florida 32827, United States*

Amanda Cox − *Burnett School of Biomedical Sciences, College of Medicine, University of Central Florida, Orlando, Florida 32827, United States*

K. Kai McKinstry − *Burnett School of Biomedical Sciences, College of Medicine, University of Central Florida, Orlando, Florida 32827, United States*

Lei Zhai − *Nanotechnology Science Center, University of Central Florida, Orlando, Florida 32826, United States; Department of Materials Science and Engineering, College of Engineering and Computer Science and Department of Chemistry, College of Science, University of Central Florida, Orlando, Florida 32816, United States;* orcid.org/0000-0002-3886-2154

Complete contact information is available at: https://pubs.acs.org/10.1021/acsomega.0c05998

Author Contributions

⊥D.N. and O.F. contributed equally. The manuscript was written through contributions of all authors. D.N., O.F., D.F., Y.Y.L.S., C.F., H.G., and A.C. contributed to data acquisition. K.K.M., L.Z., and A.R.K. contributed to the experimental design and manuscript preparation. All authors have given approval to the final version of the manuscript.

Funding

Funding was provided by the Breast Cancer Research Foundation (BCRF) (BCRF-18-086).

Notes

The authors declare the following competing financial interest(s): The authors declare that A.R.K. is a shareholder in Seva Therapeutics, Inc. The other authors have no competing interests or relationships that could be construed as a potential conflict of interest.

■ ACKNOWLEDGMENTS

In addition to the grant from BCRF (A.R.K.), this work was supported by two awards from the University of Central Florida: BSBS Interdivision Research Award (A.R.K. and K.M.) and NSTC Seed Award (L.Z. and A.R.K.). Trans-endothelial transport illustrations were provided by Arianys

Flores. CTEM analysis was assisted by Rodrigo Jacamo, Essen Instruments.

■ ABBREVIATIONS

(NPs), nanoparticles; (HBPE), hyperbranched polyester polymer; (NS), normal sera; (TNBC), triple-negative breast cancer; (PEG), poly(ethylene glycol); (EPR), enhanced permeability and retention; (RBCs), red blood cells; (HCl), hydrochloric acid; (PBS), phosphate buffered saline; (NMR), nuclear magnetic resonance; (TEM), transmission electron microscopy; (MW), molecular weight; (DLS), dynamic light scattering; (PDI), polydispersity index; (CTEM), chemotaxis transendothelial migration

■ REFERENCES

(1) Nichols, J. W.; Bae, Y. H. EPR: Evidence and fallacy. *J. Controlled Release* **2014**, *190*, 451−464.
(2) Sindhwani, S.; Syed, A. M.; Ngai, J.; Kingston, B. R.; Maiorino, L.; Rothschild, J.; MacMillan, P.; Zhang, Y.; Rajesh, N. U.; Hoang, T.; Wu, J. L. Y.; Wilhelm, S.; Zilman, A.; Gadde, S.; Sulaiman, A.; Ouyang, B.; Lin, Z.; Wang, L.; Egeblad, M.; Chan, W. C. W. The entry of nanoparticles into solid tumours. *Nat. Mater.* **2020**, *19*, 566−575.
(3) Dai, Q.; Wilhelm, S.; Ding, D.; Syed, A. M.; Sindhwani, S.; Zhang, Y.; Chen, Y. Y.; MacMillan, P.; Chan, W. C. W. Quantifying the Ligand-Coated Nanoparticle Delivery to Cancer Cells in Solid Tumors. *ACS Nano* **2018**, *12*, 8423−8435.
(4) Wilhelm, S.; Tavares, A. J.; Dai, Q.; Ohta, S.; Audet, J.; Dvorak, H. F.; Chan, W. C. W. Analysis of nanoparticle delivery to tumours. *Nat. Rev. Mater.* **2016**, *1*, 16014.
(5) Owens, D. E., III; Peppas, N. A. Opsonization, biodistribution, and pharmacokinetics of polymeric nanoparticles. *Int. J. Pharm.* **2006**, *307*, 93−102.
(6) Suk, J. S.; Xu, Q.; Kim, N.; Hanes, J.; Ensign, L. M. PEGylation as a strategy for improving nanoparticle-based drug and gene delivery. *Adv. Drug Delivery Rev.* **2016**, *99*, 28−51.
(7) Hoang Thi, T. T.; Pilkington, E. H.; Nguyen, D. H.; Lee, J. S.; Park, K. D.; Truong, N. P. The Importance of Poly(ethylene glycol) Alternatives for Overcoming PEG Immunogenicity in Drug Delivery and Bioconjugation. *Polymer* **2020**, *12*, 298.
(8) Cruje, C. C.; Chithrani, D. B. Polyethylene Glycol Density and Length Affects Nanoparticle Uptake by Cancer Cells. *J. Nanomed. Res.* **2014**, *1*, No. 00006.
(9) Breznica, P.; Koliqi, R.; Daka, A. A review of the current understanding of nanoparticles protein corona composition. *Med. Pharm. Rep.* **2020**, *93*, 342−350.
(10) Cai, R.; Chen, C. The Crown and the Scepter: Roles of the Protein Corona in Nanomedicine. *Adv. Mater.* **2019**, *31*, No. e1805740.
(11) Hu, C.-M. J.; Zhang, L.; Aryal, S.; Cheung, C.; Fang, R. H.; Zhang, L. Erythrocyte membrane-camouflaged polymeric nanoparticles as a biomimetic delivery platform. *Proc. Natl. Acad. Sci. U. S. A.* **2011**, *108*, 10980−10985.
(12) Jiménez-Jiménez, C.; Manzano, M.; Vallet-Regí, M. Nanoparticles Coated with Cell Membranes for Biomedical Applications. *Biology* **2020**, *9*, 406.
(13) Li, R.; He, Y.; Zhang, S.; Qin, J.; Wang, J. Cell membrane-based nanoparticles: a new biomimetic platform for tumor diagnosis and treatment. *Acta Pharm. Sin. B* **2018**, *8*, 14−22.
(14) Pereira-Silva, M.; Santos, A. C.; Conde, J.; Hoskins, C.; Concheiro, A.; Alvarez-Lorenzo, C.; Veiga, F. Biomimetic cancer cell membrane-coated nanosystems as next-generation cancer therapies. *Expert Opin. Drug Delivery* **2020**, *17*, 1515−1518.
(15) Xu, C.-H.; Ye, P.-J.; Zhou, Y.-C.; He, D.-X.; Wei, H.; Yu, C.-Y. Cell membrane-camouflaged nanoparticles as drug carriers for cancer therapy. *Acta Biomater.* **2020**, *105*, 1−14.
(16) He, Z.; Zhang, Y.; Feng, N. Cell membrane-coated nanosized active targeted drug delivery systems homing to tumor cells: A review. *Mater. Sci. Eng. C* **2020**, *106*, 110298.
(17) Ai, X.; Hu, M.; Wang, Z.; Zhang, W.; Li, J.; Yang, H.; Lin, J.; Xing, B. Recent Advances of Membrane-Cloaked Nanoplatforms for Biomedical Applications. *Bioconjugate Chem.* **2018**, *29*, 838−851.
(18) Elechalawar, C. K.; Hossen, M. N.; McNally, L.; Bhattacharya, R.; Mukherjee, P. Analysing the nanoparticle-protein corona for potential molecular target identification. *J. Controlled Release* **2020**, *322*, 122−136.
(19) Caputo, D.; Papi, M.; Coppola, R.; Palchetti, S.; Digiacomo, L.; Caracciolo, G.; Pozzi, D. A protein corona-enabled blood test for early cancer detection. *Nanoscale* **2017**, *9*, 349−354.
(20) Pustulka, S. M.; Ling, K.; Pish, S. L.; Champion, J. A. Protein Nanoparticle Charge and Hydrophobicity Govern Protein Corona and Macrophage Uptake. *ACS Appl. Mater. Interfaces* **2020**, *12*, 48284−48295.
(21) Carr, A. C.; Khaled, A. S.; Bassiouni, R.; Flores, O.; Nierenberg, D.; Bhatti, H.; Vishnubhotla, P.; Perez, J. M.; Santra, S.; Khaled, A. R. Targeting chaperonin containing TCP1 (CCT) as a molecular therapeutic for small cell lung cancer. *Oncotarget* **2017**, *8*, 110273−110288.
(22) Boohaker, R. J.; Zhang, G.; Lee, M. W.; Nemec, K. N.; Santra, S.; Perez, J. M.; Khaled, A. R. Rational development of a cytotoxic peptide to trigger cell death. *Mol. Pharmaceutics* **2012**, *9*, 2080−2093.
(23) Santra, S.; Kaittanis, C.; Perez, J. M. Aliphatic hyperbranched polyester: a new building block in the construction of multifunctional nanoparticles and nanocomposites. *Langmuir* **2010**, *26*, 5364−5373.
(24) Kamaly, N.; Yameen, B.; Wu, J.; Farokhzad, O. C. Degradable Controlled-Release Polymers and Polymeric Nanoparticles: Mechanisms of Controlling Drug Release. *Chem. Rev.* **2016**, *116*, 2602−2663.
(25) Ahmed, T. A.; Aljaeid, B. M. Preparation, characterization, and potential application of chitosan, chitosan derivatives, and chitosan metal nanoparticles in pharmaceutical drug delivery. *Drug Des., Dev. Ther.* **2016**, *10*, 483−507.
(26) Wu, W.-X.; Liu, Z. Novozym 435-Catalyzed Synthesis of Well-Defined Hyperbranched Aliphatic Poly(*β*-thioether ester). *Molecules* **2020**, *25*, 687.
(27) Liu, Y.; Wang, J.; Xiong, Q.; Hornburg, D.; Tao, W.; Farokhzad, O. C. Nano-Bio Interactions in Cancer: From Therapeutics Delivery to Early Detection. *Acc. Chem. Res.* **2021**, *54*, 291−301.
(28) Heckert, B.; Banerjee, T.; Sulthana, S.; Naz, S.; Alnasser, R.; Thompson, D.; Normand, G.; Grimm, J.; Perez, J. M.; Santra, S. Design and Synthesis of New Sulfur-Containing Hyperbranched Polymer and Theranostic Nanomaterials for Bimodal Imaging and Treatment of Cancer. *ACS Macro Lett.* **2017**, *6*, 235−240.
(29) Flores, O.; Santra, S.; Kaittanis, C.; Bassiouni, R.; Khaled, A. S.; Khaled, A. R.; Grimm, J.; Perez, J. M. PSMA-Targeted Theranostic Nanocarrier for Prostate Cancer. *Theranostics* **2017**, *7*, 2477−2494.
(30) Bassiouni, R.; Nemec, K. N.; Iketani, A.; Flores, O.; Showalter, A.; Khaled, A. S.; Vishnubhotla, P.; Sprung, R. W., Jr.; Kaittanis, C.; Perez, J. M.; Khaled, A. R. Chaperonin Containing TCP-1 Protein Level in Breast Cancer Cells Predicts Therapeutic Application of a Cytotoxic Peptide. *Clin. Cancer Res.* **2016**, *22*, 4366−4379.
(31) Lee, M. W.; Bassiouni, R.; Sparrow, N. A.; Iketani, A.; Boohaker, R. J.; Moskowitz, C.; Vishnubhotla, P.; Khaled, A. S.; Oyer, J.; Copik, A.; Fernandez-Valle, C.; Perez, J. M.; Khaled, A. R. The CT20 peptide causes detachment and death of metastatic breast cancer cells by promoting mitochondrial aggregation and cytoskeletal disruption. *Cell Death Dis.* **2014**, *5*, No. e1249.
(32) Santra, S.; Kaittanis, C.; Perez, J. M. Cytochrome C encapsulating theranostic nanoparticles: a novel bifunctional system for targeted delivery of therapeutic membrane-impermeable proteins to tumors and imaging of cancer therapy. *Mol. Pharmaceutics* **2010**, *7*, 1209−1222.
(33) Danaei, M.; Dehghankhold, M.; Ataei, S.; Hasanzadeh Davarani, F.; Javanmard, R.; Dokhani, A.; Khorasani, S.; Mozafari,

https://dx.doi.org/10.1021/acsomega.0c05998
ACS Omega 2021, 6, 5591−5606

M. R. Impact of Particle Size and Polydispersity Index on the Clinical Applications of Lipidic Nanocarrier Systems. *Pharmaceutics* **2018**, *10*, 57.
(34) Wooley, K. L.; Hawker, C. J.; Lee, R.; Fréchet, J. M. J. One-Step Synthesis of Hyperbranched Polyesters. Molecular Weight Control and Chain End Functionalization. *Polym. J.* **1994**, *26*, 187−197.
(35) Elsabahy, M.; Wooley, K. L. Design of polymeric nanoparticles for biomedical delivery applications. *Chem. Soc. Rev.* **2012**, *41*, 2545−2561.
(36) Bharathi, P.; Moore, J. S. Controlled synthesis of hyperbranched polymers by slow monomer addition to a core. *Macromolecules* **2000**, *33*, 3212−3218.
(37) Zheng, T.; Crews, J.; McGill, J. L.; Dhume, K.; Finn, C.; Strutt, T.; McKinstry, K. K.; Huo, Q. A Single-Step Gold Nanoparticle-Blood Serum Interaction Assay Reveals Humoral Immunity Development and Immune Status of Animals from Neonates to Adults. *ACS Infect. Dis.* **2019**, *5*, 228−238.
(38) Zheng, T.; Finn, C.; Parrett, C. J.; Dhume, K.; Hwang, J. H.; Sidhom, D.; Strutt, T. M.; Li Sip, Y. Y.; McKinstry, K. K.; Huo, Q. A Rapid Blood Test To Determine the Active Status and Duration of Acute Viral Infection. *ACS Infect. Dis.* **2017**, *3*, 866−873.
(39) Zhang, T.; Tang, M.; Yao, Y.; Ma, Y.; Pu, Y. MWCNT interactions with protein: surface-induced changes in protein adsorption and the impact of protein corona on cellular uptake and cytotoxicity. *Int. J. Nanomed.* **2019**, *Volume 14*, 993−1009.
(40) Lindman, S.; Lynch, I.; Thulin, E.; Nilsson, H.; Dawson, K. A.; Linse, S. Systematic investigation of the thermodynamics of HSA adsorption to N-iso-propylacrylamide/N-tert-butylacrylamide copolymer nanoparticles. Effects of particle size and hydrophobicity. *Nano Lett.* **2007**, *7*, 914−920.
(41) Berrecoso, G.; Crecente-Campo, J.; Alonso, M. J. Unveiling the pitfalls of the protein corona of polymeric drug nanocarriers. *Drug Delivery Transl. Res.* **2020**, *10*, 730−750.
(42) Yu, L.; Xu, M.; Xu, W.; Xiao, W.; Jiang, X.-H.; Wang, L.; Gao, H. Enhanced Cancer-targeted Drug Delivery Using Precoated Nanoparticles. *Nano Lett.* **2020**, 8903.
(43) Hrkach, J.; von Hoff, D.; Mukkaram Ali, M.; Andrianova, E.; Auer, J.; Campbell, T.; de Witt, D.; Figa, M.; Figueiredo, M.; Horhota, A.; Low, S.; McDonnell, K.; Peeke, E.; Retnarajan, B.; Sabnis, A.; Schnipper, E.; Song, J. J.; Song, Y. H.; Summa, J.; Tompsett, D.; Troiano, G.; van Geen Hoven, T.; Wright, J.; LoRusso, P.; Kantoff, P. W.; Bander, N. H.; Sweeney, C.; Farokhzad, O. C.; Langer, R.; Zale, S. Preclinical development and clinical translation of a PSMA-targeted docetaxel nanoparticle with a differentiated pharmacological profile. *Sci. Transl. Med.* **2012**, *4*, 128ra39.
(44) van Eerden, R. A. G.; Mathijssen, R. H. J.; Koolen, S. L. W. Recent Clinical Developments of Nanomediated Drug Delivery Systems of Taxanes for the Treatment of Cancer. *Int. J. Nanomed.* **2020**, *15*, 8151−8166.
(45) Yang, T.; Cui, F.-D.; Choi, M.-K.; Cho, J.-W.; Chung, S.-J.; Shim, C.-K.; Kim, D.-D. Enhanced solubility and stability of PEGylated liposomal paclitaxel: in vitro and in vivo evaluation. *Int. J. Pharm.* **2007**, *338*, 317−326.
(46) Kim, S. C.; Kim, D. W.; Shim, Y. H.; Bang, J. S.; Oh, H. S.; Kim, S. W.; Seo, M. H. In vivo evaluation of polymeric micellar paclitaxel formulation: toxicity and efficacy. *J. Controlled Release* **2001**, *72*, 191−202.
(47) Fujiwara, Y.; Mukai, H.; Saeki, T.; Ro, J.; Lin, Y.-C.; Nagai, S. E.; Lee, K. S.; Watanabe, J.; Ohtani, S.; Kim, S. B.; Kuroi, K.; Tsugawa, K.; Tokuda, Y.; Iwata, H.; Park, Y. H.; Yang, Y.; Nambu, Y. A multi-national, randomised, open-label, parallel, phase III non-inferiority study comparing NK105 and paclitaxel in metastatic or recurrent breast cancer patients. *Br. J. Cancer* **2019**, *120*, 475−480.
(48) Desai, N.; Trieu, V.; Yao, Z.; Louie, L.; Ci, S.; Yang, A.; Tao, C.; De, T.; Beals, B.; Dykes, D.; Noker, P.; Yao, R.; Labao, E.; Hawkins, M.; Soon-Shiong, P. Increased antitumor activity, intratumor paclitaxel concentrations, and endothelial cell transport of cremophor-free, albumin-bound paclitaxel, ABI-007, compared with cremophor-based paclitaxel. *Clin. Cancer Res.* **2006**, *12*, 1317−1324.
(49) Rezaei, G.; Daghighi, S. M.; Raoufi, M.; Esfandyari-Manesh, M.; Rahimifard, M.; Mobarakeh, V. I.; Kamalzare, S.; Ghahremani, M. H.; Atyabi, F.; Abdollahi, M.; Rezaee, F.; Dinarvand, R. Synthetic and biological identities of polymeric nanoparticles influencing the cellular delivery: An immunological link. *J. Colloid Interface Sci.* **2019**, *556*, 476−491.
(50) Papini, E.; Tavano, R.; Mancin, F. Opsonins and Dysopsonins of Nanoparticles: Facts, Concepts, and Methodological Guidelines. *Front. Immunol.* **2020**, *11*, 567365.
(51) Fedeli, C.; Segat, D.; Tavano, R.; Bubacco, L.; De Franceschi, G.; de Laureto, P. P.; Lubian, E.; Selvestrel, F.; Mancin, F.; Papini, E. The functional dissection of the plasma corona of SiO_2-NPs spots histidine rich glycoprotein as a major player able to hamper nanoparticle capture by macrophages. *Nanoscale* **2015**, *7*, 17710−17728.
(52) Ju, Y.; Kelly, H. G.; Dagley, L. F.; Reynaldi, A.; Schlub, T. E.; Spall, S. K.; Bell, C. A.; Cui, J.; Mitchell, A. J.; Lin, Z.; Wheatley, A. K.; Thurecht, K. J.; Davenport, M. P.; Webb, A. I.; Caruso, F.; Kent, S. J. Person-Specific Biomolecular Coronas Modulate Nanoparticle Interactions with Immune Cells in Human Blood. *ACS Nano* **2020**, *14*, 15723−15737.
(53) Ndumiso, M.; Buchtová, N.; Husselmann, L.; Mohamed, G.; Klein, A.; Aucamp, M.; Canevet, D.; D'Souza, S.; Maphasa, R. E.; Boury, F.; Dube, A. Comparative whole corona fingerprinting and protein adsorption thermodynamics of PLGA and PCL nanoparticles in human serum. *Colloids Surf., B* **2020**, *188*, 110816.
(54) Cagliani, R.; Gatto, F.; Bardi, G. Protein Adsorption: A Feasible Method for Nanoparticle Functionalization? *Materials* **2019**, *12*, 1991.
(55) Qin, M.; Zhang, J.; Li, M.; Yang, D.; Liu, D.; Song, S.; Fu, J.; Zhang, H.; Dai, W.; Wang, X.; Wang, Y.; He, B.; Zhang, Q. Proteomic analysis of intracellular protein corona of nanoparticles elucidates nano-trafficking network and nano-bio interactions. *Theranostics* **2020**, *10*, 1213−1229.
(56) Sugo, K.; Ebara, M. A simple spectrophotometric evaluation method for the hydrophobic anticancer drug paclitaxel. *PeerJ Anal. Chem.* **2020**, *2*, No. e3.

https://dx.doi.org/10.1021/acsomega.0c05998
ACS Omega 2021, 6, 5591−5606